ISSN 1590-2595
Anno 2014_Numero 119

Hyperspectral spaceborne, airborne and ground measurements campaign on Mt. Etna: multi data acquisitions in the frame of Prisma Mission (ASI-AGI Project n. I/016/11/0)

Quaderni di Geofisica

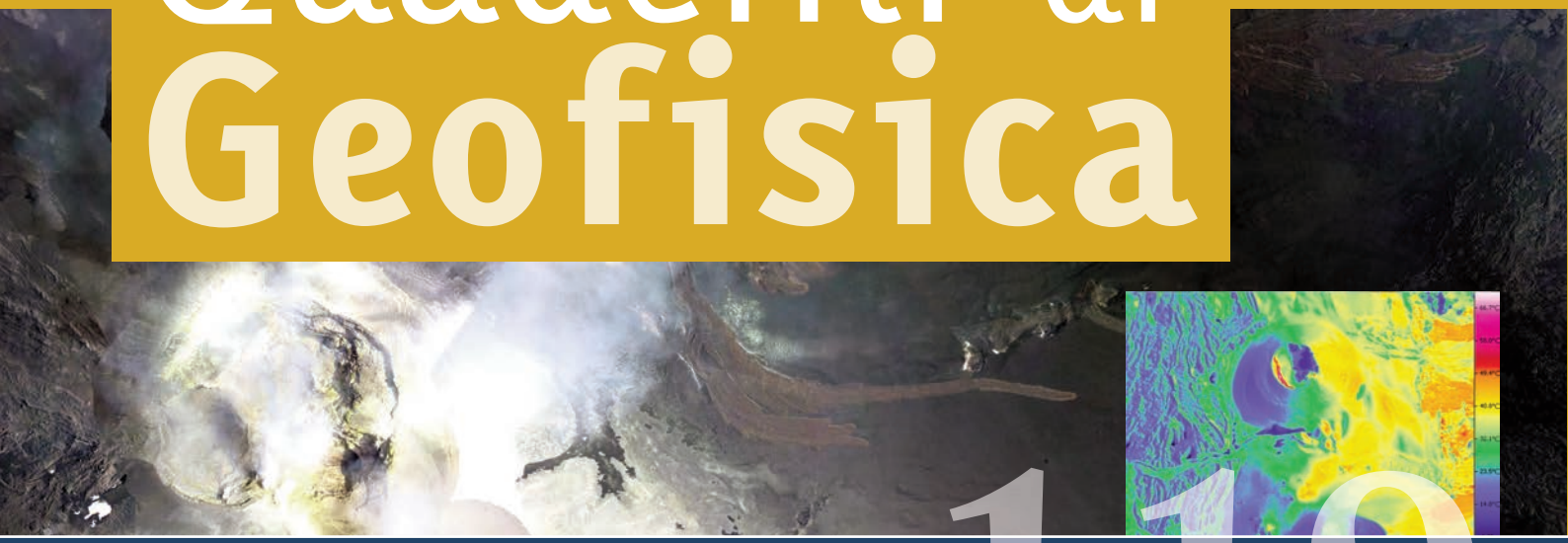

119

Istituto Nazionale di
Geofisica e Vulcanologia

Quaderni di Geofisica

Segreteria di Redazione
Francesca Di Stefano
Tel. +39 06 51860068
Fax +39 06 36915617
Rossella Celi
Tel. +39 095 7165844

redazionecen@ingv.it

ISSN 1590-2595
Anno 2014_Numero 119

Hyperspectral spaceborne, airborne and ground measurements campaign on Mt. Etna: multi data acquisitions in the frame of Prisma Mission (ASI-AGI Project n. I/016/11/0)

La campagna di misure aeree, da satellite e di terra sull'Etna: acquisizione "multi-data" nell'ambito della missione PRISMA (progetto ASI-AGI n. I/016/11/0)

Laura Colini[1], Claudia Spinetti[1], Stefania Amici[1], Maria Fabrizia Buongiorno[1], Tommaso Caltabiano[2], Fawzi Doumaz[1], Massimiliano Favalli[3], Salvatore Giammanco[2], Ilaria Isola[3], Alessandro La Spina[2], Valerio Lombardo[1], Francesco Mazzarini[3], Massimo Musacchio[1], Marco Neri[2], Giuseppe Salerno[2],Malvina Silvestri[1], Sergio Teggi[4], Valentina Sarli[5], Paolo Cafaro[6], Marco Mancini[6], Salvatore D'Andrea[6], Gabriele Curci[7], Cristina Ananasso[8]

[1]**INGV** (Istituto Nazionale di Geofisica e Vulcanologia, Centro Nazionale Terremoti)

[2]**INGV** (Istituto Nazionale di Geofisica e Vulcanologia, Sezione di Catania - Osservatorio Etneo)

[3]**INGV** (Istituto Nazionale di Geofisica e Vulcanologia, Sezione di Pisa)

[4]**Università di Modena e Reggio Emilia**

[5]**CGIAM** (Centro di Geomorfologia Integrata dell'Area del Mediterraneo - Potenza)

[6]**Comando Generale del Corpo delle Capitanerie di Porto – Guardia Costiera** (Roma)

[7]**Università degli Studi dell'Aquila** (CETEMPS - Dipartimento Scienze Fisiche e Chimiche)

[8]**Agenzia Spaziale Italiana**

in copertina Mosaico delle immagini aeree riprese dalla camera ad alta risoluzione Digicam H-39 della zona sommitale dell'Etna. Nel riquadro, l'immagine in temperatura acquisita nei canali IR (particolare)

Hyperspectral spaceborne, airborne and ground measurements campaign on Mt. Etna: multi data acquisitions in the frame of Prisma Mission (ASI-AGI Project n. I/016/11/0)

In the frame of the Italian Space Agency (ASI) Hyperspectral Mission PRISMA (Precursore IperSpettrale della Missione Applicativa), the Istituto Nazionale di Geofisica e Vulcanologia (INGV) is coordinating the scientific project ASI-AGI (Analisi Sistemi Iperspettrali per le Applicazioni Geofisiche Integrate) to develop specific algorithms and products for various geophysical applications. The data validation and calibration activities have been focused on three active volcanic areas located in Sicily: Mt. Etna, Paternò and Ciclopi islands.
From June 23 until 27, 2012 INGV and the project partners have organized an airborne and ground campaign over the selected test sites covering different surface targets. The airborne data were acquired by using a SPECIM sensor working in the VNIR-SWIR range and jointed to an airborne laser scanner and a thermal camera. The ground campaign has allowed to collect several datasets using two portable spectroradiometer (Fieldspec), two portable Fourier Transform InfraRed spectrometer (FTIR), a ground laser scanner, a thermal camera and a TIR thermometer. Moreover, in order to acquire local atmospheric parameters a sun photometer and a meteorological station have been used as well as further meteorological information have been furnished by CETEMPS L'Aquila University. During the airborne and ground campaign the contemporaneous acquisitions of Hyperion and ASTER have allowed to extract a suitable data set that will be used to simulate PRISMA data and to develop and test the proposed algorithms for a large number of applications regarding for example land cover and agriculture, water quality monitoring, surface hydrology, urban areas monitoring, geology, security, desertification, territory monitoring to support to natural hazard management, atmosphere monitoring for its optical and spectral characterization, carbon cycle.

Nell'ambito della Missione Iperspettrale PRISMA (Precursore IperSpettrale della Missione Applicativa) dell'Agenzia Spaziale Italiana (ASI), l'Istituto Nazionale di Geofisica e Vulcanologia (INGV) sta coordinando il progetto scientifico ASI-AGI (Analisi Sistemi Iperspettrali per le Applicazioni Geofisiche Integrate) per sviluppare algoritmi e prodotti specifici per diverse applicazioni geofisiche. Le attività di validazione e calibrazione dei dati sono state focalizzate su tre aree vulcaniche attive individuate in Sicilia: Mt. Etna, area di Paternò e isole dei Ciclopi. Dal 23 al 27 giugno 2012, l'INGV ed i partner del progetto hanno organizzato una campagna di volo e di terra sui siti di prova scelti coprendo diverse tipologie di superfici. I dati aerei sono stati acquisiti utilizzando un sensore SPECIM operante nell'intervallo VNIR-SWIR e collegato ad un laser scanner aereo e ad una camera termica. La campagna di terra ha permesso di raccogliere numerosi datasets mediante l'utilizzo di due spettroradiometri portatili (Fieldspec), di due spettrometri portatili FTIR, di un laser scanner a terra, di una camera termica e di un termometro TIR. Inoltre, al fine di acquisire i parametri atmosferici locali, sono stati utilizzati un fotometro solare ed una stazione meteorologica, oltre alle informazioni meteorologiche fornite dal CETEMPS dell'Università dell'Aquila. Durante la campagna aerea e di terra le acquisizioni contemporanea di Hyperion e ASTER hanno permesso di estrarre un set di dati che permetteranno di simulare i dati PRISMA e di sviluppare e testare gli algoritmi proposti per un gran numero di applicazioni quali per esempio land cover e agricoltura, monitoraggio della qualità delle acque, idrologia superficiali, monitoraggio delle aree urbane, geologia, sicurezza, desertificazione, monitoraggio del territorio a supporto della gestione dei rischi naturali, monitoraggio dell'atmosfera per la caratterizzazione spettrale e ottica, ciclo del carbonio.

Introduction

Data acquired by imaging spectrometers and multispectral imagers are able to provide important information in geophysical processes as volcanic activity during both quiescent and active periods. In particular, the infrared region of the EM spectrum is suitable for investigations of the compositions of volcanic plumes and clouds and to characterize the thermal properties and conditions of volcanic surfaces. Thermal anomalies in both quiescent and active periods could be monitored using SWIR-TIR images. VIS-TIR bands could be used to analyze the mineralogical composition and weathering processes of lava flows and other volcanic products since they are usually subject to rapid weathering in humid climates and, therefore, the vegetation regrowth on new volcanic deposits (starting from lichens) is an important indication of the age of lava flows thus it represents an important element in risk analysis procedures. All these studies involve the use of high spatial and spectral resolution. EO-1-Hyperion space sensor has furnished hyperspectral images worldwide and has demonstrated the importance of imaging spectrometers to monitor volcanic phenomena especially in conjunction with ASTER images that are able to cover the TIR spectral range. The HyspIRI mission represents a fundamental step forward in integrating VIS-TIR imagers to benefit a large number of scientific studies and operational activities. In the frame of the Italian Space Agency (ASI) Hyperspectral mission PRISMA, INGV is coordinating scientific studies for geophysical applications. Considering the spectral range covered by the PRISMA sensor (0.4-2.5μm, 30 m spatial resolution) and the contemporaneous acquisition of panchromatic camera at 5 m spatial resolution, a number of products are being developed for scientific applications in particular they will regard the thermal structure of lava flows and forest fires, volcanic gas emission (CO_2, CH_4) and surface material classification based on spectral analysis and development of data fusion techniques. Moreover the proposed activities will include systematic measurements on a calibration/validation test sites as Mt. Etna and a large calibration site located in the Algeria desert. This paper focuses on the detailed description of the campaign with particular regard to the measurements performed and to the instruments used.

1. PRISMA mission characteristics

PRISMA (Precursore IperSpettrale della Missione Applicativa) is a pre-operative small Italian hyperspectral mission aiming to monitor and characterize the earth surface through the combination of an hyperspectral and a panchromatic sensor (Figure 1). In this context PRISMA target is to qualify the technology, contribute to develop applications and provide products to institutional and scientific users for environmental observation and risk management.

1.1 Mission objectives

- In orbit qualification of an Italian hyperspectral/panchromatic camera (Figure 2);
- implementation of a pre-operative mission, with demonstrative/technological features;
- validation of end-to-end data processing able to develop new applications based on high spectral resolution images for Earth observation and to manage the environmental risks;
- capitalization of ASI heritage, considering the Hypseo mission and the Italian-Canadian Joint Hyperspectral Mission (JHM) studies.

Figure 1 ASI PRISMA mission characteristics.
Figura 1 Caratteristiche della missione ASI-PRISMA.

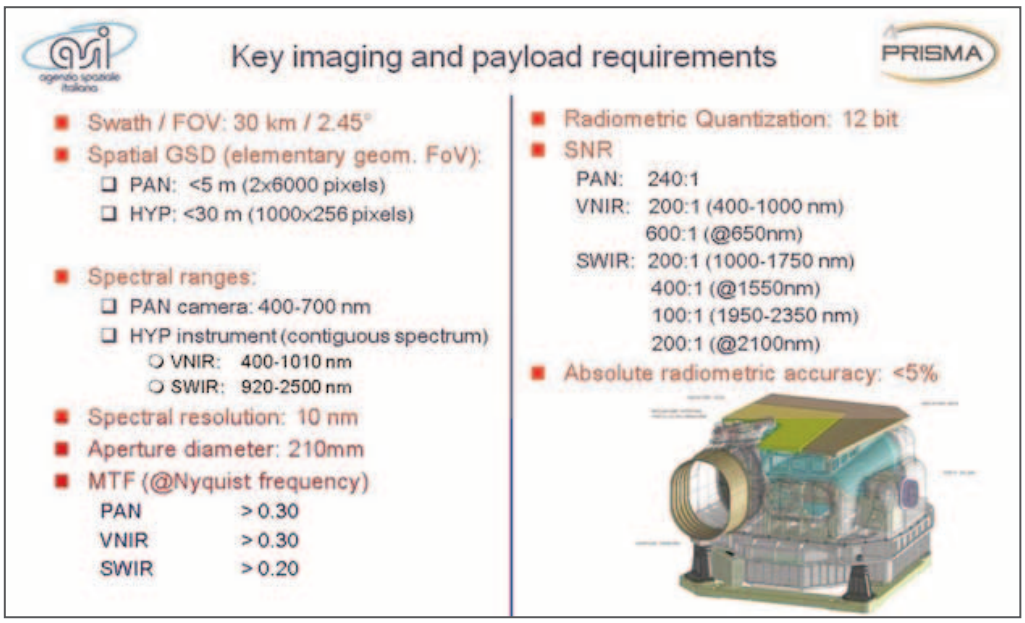

Figure 2 ASI PRISMA key imaging and payload requirements.
Figura 2 Caratteristiche del sensore e requisiti di payload di ASI PRISMA.

ASI has given responsibility for the performance of these tasks to the Raggruppamento Temporaneo d'Imprese (RTI) (Temporary Industrial Group) made up of Carlo Gavazzi Space, S.p.A as the procurer and Selex-Galileo Avionica S.p.A and Oerlikon Contraves Rheinmetall Italia S.p.A as principal contractors.

This group manages a team that involves the participation of other important Italian industries working in the sector. The contract will assign the contractor the "end-to-end" responsibility for the development and production of the system to the in-orbit commissioning (Phase B2/C/D/E1).

1.2 ASI-AGI Project

In the latest decades the technological development of imaging spectrometers, both on airborne and spaceborne platforms, has promoted a great number of applications. In particular, several studies have analyzed the interaction between Earth surface and atmosphere. Because of the increasing interest in developing applications, the Italian Space Agency (ASI) is carrying on the Hyperspectral mission PRISMA (Precursore IperSpettrale della Missione Applicativa) that will ensure the continuity of NASA and ESA missions HYPERION and CHRIS PROBA, respectively. PRISMA will first cover the Euro-Mediterranean regions. In 2009 ASI sent out a call for

TITLE	Name of the institute	
Development of algorithms and products for applications in agriculture and land monitoring to support the PRISMA mission (SAP 4 PRISMA)	Istituto di Metodologie per l'Analisi Ambientale IMAA CNR	Vincenzo Cuomo
Singergistic use of PRISMA products with high resolution meteo-chemistry simulations and their validation from ground and satellites (PRIMES)	CETEMPS - Univ. de L'Aquila	Guido Visconti
Hyperspectral systems analisys for integrated geophysical applications (ASI-AGI)	Istituto Nazionale di Geofisica e Vulcanologia (INGV)	Fabrizia Buongiorno
Advanced methodologies for analysis, integration and optimization of PRISMA level 1 and 2 products - OPTIMA -	Istituto di Fisica Applicata Nello Carrara (IFAC -CNR)	Ivan Pippi
Coasts and Lake Assessment and Monitoring by PRISMA HYperspectral Mission (CLAM PHYM)	Institute of Marine Sciences (ISMAR - CNR)	Luigi Alberotanza

Table 1 Showing the PRISMA scientific studies funded by ASI.
Tabella 1 Studi scientifici su PRISMA finanziati da ASI.

proposal to support scientific studies (Table 1) and to promote the PRISMA science team. and a number of applications, ASI-AGI (**A**nalisi **S**istemi **I**perspettrali per le **A**pplicazioni **G**eofisiche **I**ntegrate) is one of the selected projects. The projects started in April 2011 and they will be closed in April 2015 in order to be aligned to the development phase of PRISMA mission whose launch is scheduled for 2016.

The ASI AGI project focuses on geophysical and geological applications such as improving the scientific understanding of natural phenomena as volcanic activity and forest fires and developing innovative techniques based on PRISMA image spectroscopy characteristics combining an hyperspectral and a panchromatic data.

ASI-AGI project is organized in 4 main tasks and focuses on the objectives listed below:

- optimize the hyperspectral and panchromatic contribute to study geophysical phenomena;
- consolidate the use of hyperspectral data in a number of geophysical applications by developing specific algorithms;
- develop a PRISMA data simulator to test the specific algorithms during the developing phases of the PRISMA mission;
- improve the atmospheric correction procedures for hyperspectral data to achieve more precise estimation of the ground radiance and reflectance;
- organize CAL/VAL (calibration/validation) activities including the definition of a vicarious test site in Algeria;
- support the Italian Space Agency to verify the scientific and technical requirements of the PRISMA mission.

The ASI-AGI project team is composed by the following institutions:

- **Istituto Nazionale di Geofisica e Vulcanologia** (**INGV**), project coordinator and responsible of specific algorithms development for geophysical applications.
- **Dipartimento di Ingegneria Meccanica e Civile dell'Università degli Studi di Modena e Reggio Emilia** (DIMEC), responsibile of the Pan Sharpening techniques and atmospheric and topographic correction procedures.
- **Centro di Geomorfologia Integrata per l'Area del Mediterraneo** (**CGIAM**), responsible for the airborne data acquisition and part of the CAL/VAL activities.

2. ASI-AGI Sicily 2012 campaign overview

The CAL/VAL activities of ASI-AGI project are based on 4 specific goals:

- To organize an airborne campaign on Mt. Etna area which is the main test site for ASI-AGI project and acquire a suitable hyperspectral data set to simulate the PRISMA data and test the developed algorithms;
- To get possibly simultaneous Hyperion and ASTER data in order to use the acquired dataset to simulate HyspIRI data;
- To organize a contemporary in situ campaign to acquire surface and atmospheric parameters and validate the airborne data and complete a spectral library for Mt. Etna different lava flows;
- To define a vicarious test site in North Africa in the Algerian desert.

On June 2012 a campaign for hyperspectral images acquisition has been organized, instruments carried by aerial platform and portable instruments have been used for field measurements. A spectroradiometer Fieldspec Pro has

	GROUND ACTIVITIES	AIRBORNE AND SPACEBORNE ACQUISITION
23.06.2012	MILO Logistic activities Ground instrument TEST and Fieldspec measurements	Hyperion acquisition
24.06.2012	BRONTE Start ground measurements FieldSpec ETNA Set up sun-photometer PATERNÒ Site ispection	TEST FLIGHT BY CGIAM
25.06.2012	ETNA Thermal Camera, Unilogger, FTIR (Pian del Lago) FieldSpec (Strada Forestale and North Etna)	TERRA-ASTER Flight over ETNA Flight altitude: 5000 slm Time start: 8:00 (local)
26.06 2012	PATERNÒ FieldSpec, Unilogger, Laser Scanning	EO1- HYPERION Flight over PATERNÒ Flight altitude: 1000m slm Time start: 9:00-9:30 (local)
27.06-2012	FORNAZZE FieldSpec	

Table 2 Activities planned in the different test sites.
Tabella 2 Attività pianificate nei diversi siti test

allowed to acquire spectra of lavic materials in order to implement the spectral library of Etnean lava outcrops. INGV sections of Rome, Catania and Pisa and CGIAM company have participated to the campaign. During the campaign, satellite data have been acquired and released thanks to agreements with NASA-JPL and NASA-GODDARD.
The activities carried on during the campaign and the instruments used in the different test sites are listed in Table 2.
Due to the restriction in the project duration, the data validation and calibration activities were focused on active volcanic areas, with the following test site selection located in Sicily (Italy): Mt. Etna area, Paternò "Salinelle" area and Ciclopi islands.

3. Airborne campaign

The airborne campaign was carried out over the three selected test sites in the period 25-26 June 2012 in order to acquire hyperspectral and Lidar data according to the flight line scheduling planned by INGV and CGIAM.
The campaign was preceded by calibration and test flights performed during the two previous days.
The airborne multi-sensor platform used for the airborne surveys includes a hyperspectral system, a laser scanner, a thermal camera and a digital camera.

3.1 Airborne flight lines scheduling

The scheduling of the flight lines has been planned in advance taking into account different criteria such as for example the existence of flight lines executed in previous campaigns during past missions, so the new campaign covers also areas not investigated before.

3.1.1 Calibration flight on 23th June, 2012

A calibration flight was performed over the airport of Perugia in order to determine the boresight angles and to test the functionality of the sensors. The calibration flight was performed along flight lines acquired in 'cross formations' and parallel lines with a sizeable overlap, at two different altitudes (700 m a.g.l. and 1400 m a.g.l.) over an area with ground control points.
Figure 3 shows the flight lines at the two different altitudes.

3.1.2 Test flight over the Mt. Etna on 24th June 2012

The test flight over Mt. Etna was intended to verify the acquisition parameters for hyper-spectral data (e.g. integration time, frame rate, flight speed) and the flight operating conditions for the altitude needed. The flight was performed at an altitude of 4500 m a.s.l..
The flight lines are showed in Figure 4.

Figure 3 Calibration flight performed over the airport of Perugia on the 23th June 2012. The red flight lines are at an altitude of 700 m agl, the blue flight lines at 1400 m agl..
Figura 3 Volo di calibrazione eseguito sull'aereoporto di Perugia il 23 giugno 2012. Le linee in rosso si riferiscono ad una quota di volo di 700 m (sul livello del terreno) mentre le blu si riferiscono ad una quota di 1400 m (sul livello del terreno).

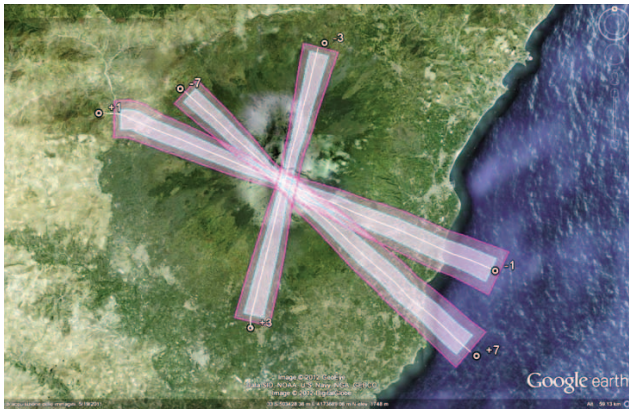

Figure 4 Flight lines (white lines), and SWIR (sky-blue) &VNIR (pink) swaths over Mt. Etna.
Figura 4 Traiettorie di volo (linee bianche), e swath relativi al SWIR (blu cielo) e al VNIR (rosa) sul Monte Etna.

3.1.3 Airborne survey over the Mt. Etna on 25th June 2012

Airborne survey over on Mt. Etna was executed on 25th June, 2012. The data were acquired along eight flight lines specified in Table 3, at the about 4500 m a.s.l., with an average velocity of about 110 knots, from about 9 a.m. to about 11 a.m. (local time). These covered the volcano craters as well as other points of interest.
The data acquired are hyperspectral, thermal and optical.
Figure 5 shows the corresponding hyperspectral swaths.

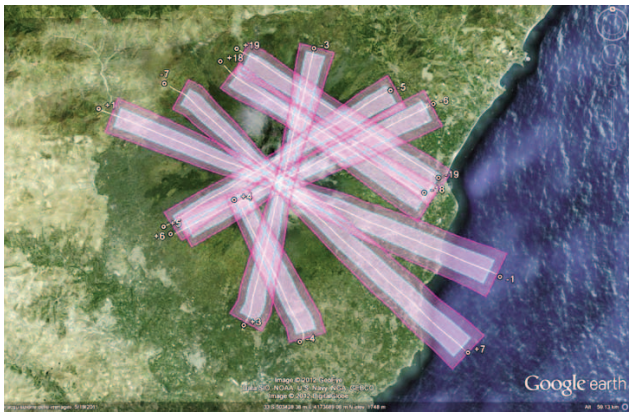

Figure 5 Flight lines (white lines), and SWIR (sky-blue swaths) & VNIR (pink swaths) swaths over Mt. Etna.
Figura 5 Traiettorie di volo (linee bianche), e swath relativi al SWIR (blu cielo) e al VNIR (rosa) sul Monte Etna.

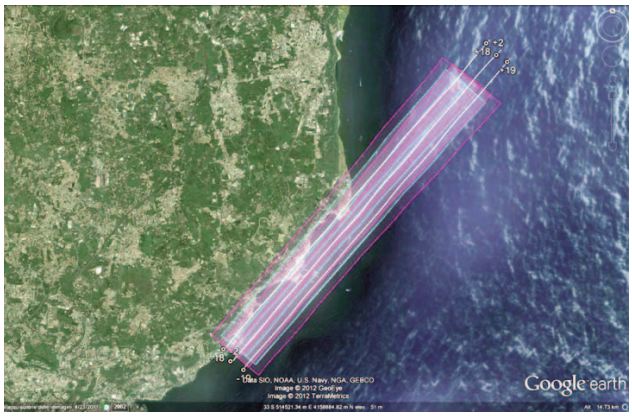

Figure 6 Flight lines (white lines), and SWIR (sky-blue) & VNIR (pink) swaths over Ciclopi Islands.
Figura 6 Traiettorie di volo (linee bianche), e swath relativi al SWIR (blu cielo) e al VNIR (rosa) sulle Isole Ciclopi.

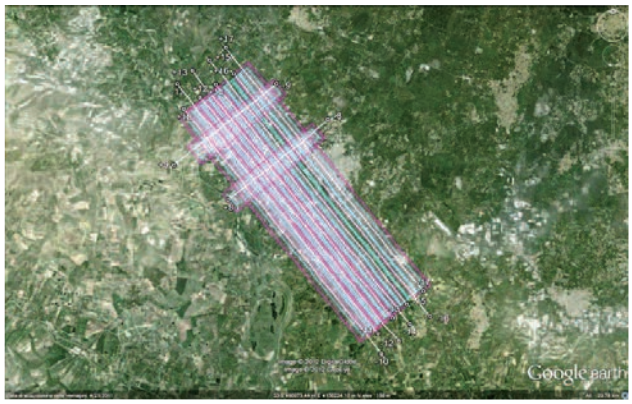

Figure 7 Flight lines (white lines), and SWIR (sky-blue) &VNIR (pink) swaths over Paternò area.
Figura 7 Traiettorie di volo (linee bianche), e swath relativi al SWIR (blu cielo) e al VNIR (rosa) sull'area di Paternò.

3.1.4 Airborne survey over the Paternò area and Ciclopi islands on 26th June, 2012

Airborne survey over Paternò area and Ciclopi islands was totally performed along thirteen flight lines, on the morning of 26th June 2012.

The mission started on the Cyclops islands in order to have a low sun elevation and therefore minimize sun glint. The data were acquired along three flight lines 18, 2 and 19, at 1000 m a. g. l., with an average velocity of about 110 knots, from about 6:45 a.m. to about 7 a.m (local time).

Subsequently, the data were acquired over Paternò area along the ten remaining flight lines (from 8 to 17) at 1000 m a. g. l., with an average velocity of about 110 knots, from about 7:15 a.m. to about 8:15 a.m.

The data acquired over both areas are hyperspectral, thermal, LiDAR and optical.

The flight lines with the coordinates of the relative start and end points and the acquisition start time are specified in Table 4.

Figures 6 and 7 show the corresponding hyperspectral swaths on Ciclopi islands and Paternò area.

3.2 Characteristics of CGIAM airborne system

The airborne multi-sensor platform used can operate in different configuration depending on number and type of sensors to be used and is installable both helicopter and fixed wings aircraft as each mission requires (Figure 8).

All the sensors are placed on a special structure with forced slots that allows an extreme stability in the relative positioning. They are synchronized via hardware and software with the Navigation System which consists of a Ground Position System (GPS) and Inertial Navigation System (INS) able to estimate the position and the attitude of all the sensors, allowing to manage and control flight parameters and sensors in real time and to collect all the useful information to geo-rectify the acquired data.

In this mission, the configuration consisted of a full waveform laser scanner, an high resolution digital camera, a hyper-spectral system of two sensors operating in VNIR and SWIR regions and a thermal camera. The aircraft used was a P68.

In the following paragraphs, the main characteristics of the sensors and the instrumentation are described.

3.3 Airborne components

The airborne system includes the following components mounted within aircraft:

- The group of the sensors (hyper-spectral system, laser scanner, thermal camera, digital camera).
- A rack for computers & storage units.
- A monitor panel.

Flight Line at 4500 m asl	Start Point		End Point		Acquisition Start time
	Lon	Lat	Lon	Lat	
19	14.9723	37.8442	15.1807	37.7370	9:11 AM
4	15.0320	37.6004	14.9618	37.7164	9:24 AM
18	14.9564	37.8257	15.1661	37.7202	9:33 AM
3	14.9720	37.6137	15.0450	37.8479	9:47 AM
7	14.8993	37.8103	15.2139	37.5830	10:03 AM
6	14.9043	37.6926	15.1717	37.7984	10:26 AM
1	14.8186	37.7925	15.2443	37.6527	10:47 AM
5	14.8904	37.6993	15.1293	37.8131	11:11 AM

Table 3 The flight lines of the airborne survey over the Mt. Etna, with the latitude and longitude coordinates (WGS84) of the corresponding acquisition start and end points, and the acquisition start time.
Tabella 3 Traiettorie di volo sul Monte Etna, con le coordinate Lat-Long (WGS84) dei corrispondenti punti di inizio e fine, e tempo di inizio acquisizione.

Flight Line at 1000 m agl	Start Point		End Point		Acquisition Start time
	Lon	Lat	Lon	Lat	
18	15.2082	37.6078	15.1408	37.5457	6:46 AM
2	15.2112	37.6058	15.1438	37.5437	6:54 AM
19	15.2140	37.6038	15.1466	37.5417	7:03 AM
10	14.9179	37.5100	14.8440	37.5824	7:14 AM
11	14.8473	37.5845	14.9212	37.5121	7:21 AM
12	14.9244	37.5142	14.8505	37.5866	7:27 AM
13	14.8538	37.5887	14.9277	37.5163	7:34 AM
14	14.9309	37.5184	14.8570	37.5908	7:40 AM
15	14.8602	37.5929	14.9341	37.5205	7:46 AM
16	14.9374	37.5226	14.8635	37.5950	7:52 AM
17	14.8667	37.5971	14.9406	37.5247	8:02 AM
8	14.8958	37.5759	14.8626	37.5548	8:10 AM
9	14.8477	37.5709	14.8793	37.5910	8:16 AM

Table 4 The flight lines of the airborne survey over the Ciclopi islands and Paternò area, with the latitude and longitude coordinates (WGS84) of the corresponding acquisition start and end points, and the acquisition start time.
Tabella 4 Traiettorie di volo sul Monte Etna, con le coordinate Lat-Long (WGS84) dei corrispondenti punti di inizio e fine, e tempo di inizio acquisizione.

While, the GPS receiver and a fiber optic sensor (FODIS) measuring downwelling light are mounted on the aircraft roof.

The group of the sensors whose main characteristics are described singly in the following sections, are fixed together an inertial measurement unit (IMU) on a non-deformable rigid aluminum plate (Figure 9).

The mounting of the group of sensors and the Rack for Computers & Storage units on fixed-wing aircraft is made fixing a MDF (medium density fiberboard) and aluminum support respectively to the cabin floor using the equipped fixing points. On these supports are installed dampers in connection with the aluminum plate and the rack.

The Rack for Computers & Storage units includes computers with storage units for every sensors and the following systems:

- The AEROControl system to determine position (x, y, z) and attitude (roll, pitch, heading) of the sensors with high precision, to give real-time navigation parameters to Computer Controlled Navigation System (CCNS) and to store the navigation data for the following step

of data processing. The AEROControl integrates the 24-channel L1/L2 GPS receiver working at 2 Hz and the Inertial Measurement Unit (IMU-IId) built by optical fiber gyroscopes and accelerometers with a 256Hz sampling frequency.

Figure 8 The multi-sensors platform installed on helicopter (on the top) and fixed wings aircraft (on the bottom).
Figura 8 Piattaforma multi-sensore istallata su un elicottero (in alto), e fissata sulle ali di un aereomobile (in basso).

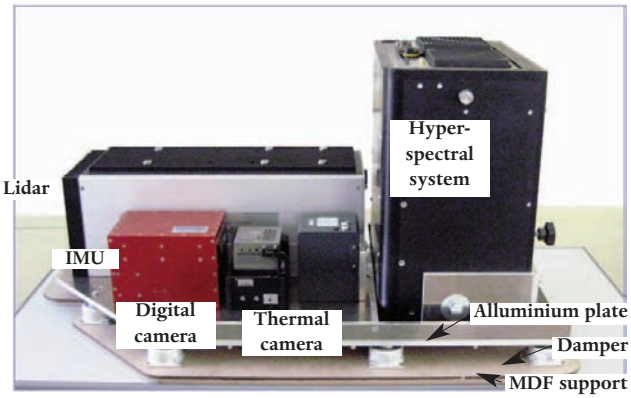

Figure 9 The multi-sensor platform with the group of sensors mounted on an aluminum plate.
Figura 9 Piattaforma multi-sensore con il gruppo di sensori montati su una piastra di alluminio.

- The Computer Controlled Navigation System (CCNS) that is a guidance, positioning and sensor management system using AEROControl data. It consists of a Central Computer Unit (CCU), a command and display unit.

The monitor panel represented in Figure 10 groups the control and display units of every sensor and the monitor of CCNS. The panel is mounted by means of a dedicated clamp or support (Figure 11).

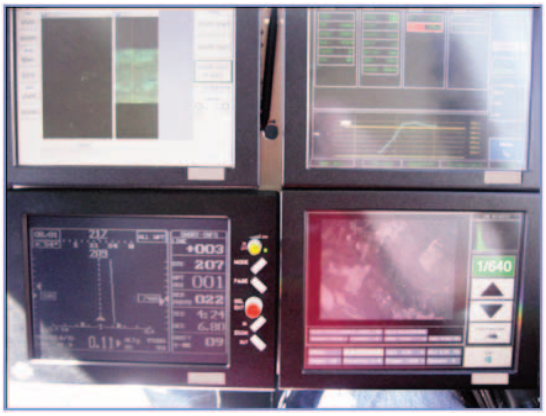

Figure 10 Monitor panel during a airborne survey.
Figura 10 Pannello di monitoraggio durante un rilevo aereo.

Figure 11 Rack for Computers & Storage units installed on aircraft.
Figura 11 Sistema di Storage istallato sull'aereo.

Hyperspectral camera

The hyperspectral system is a pushbroom scanning system that consists of two spectrophotometers operating in VNIR (from 0.4 m to 1.0 m) and SWIR (from 1.0 m to 2.5 m) spectral ranges (see Figure 13 and Table 5).
The VNIR sensor is an assembled system whose main parts are a spectrometer, the ImSpector V10E by Specim, and a CCD camera of image acquisition. Whereas the SWIR sensor is the ImSpectorN25E by Specim (Figure 12).

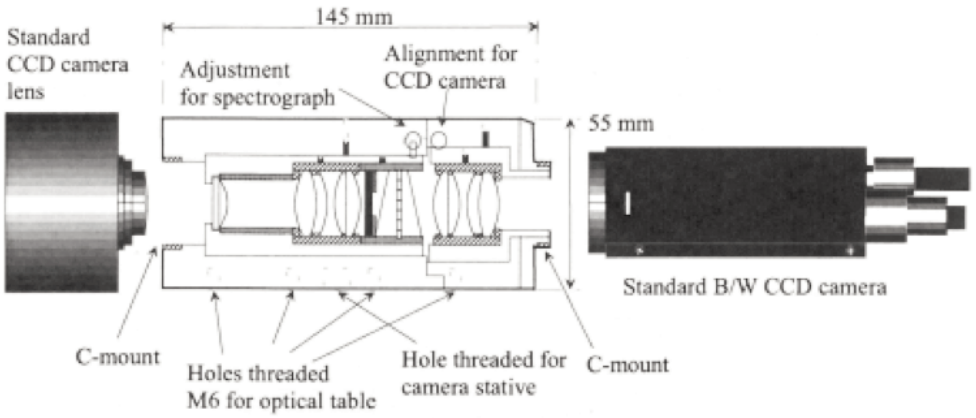

Figure 12 ImSpector Scheme.
Figura 12 Schema dell'ImSpector.

Figure 13 The two hyper-spectral sensors.
Figura 13 I due sensori iperspettrali.

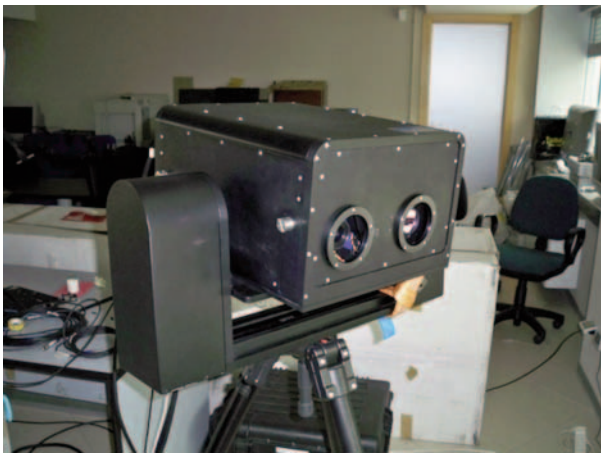

Figure 14 The hyper-spectral system mounted on a support within the rigid box.
Figura 14 Il sistema iperspettrale istallato su un supporto all'interno di una scatola rigida.

They are placed inside a rigid box (Figure 14) that can be mounted both on the airborne platform and on a support equipped with a device for vertical and horizontal movement. The system is connected to a computer that permits to adjusts the image acquisition both closing of the shutters for the dark acquisition (electronic noise) and by setting various parameters as the integration time and frame rate. Moreover, the hyper-spectral system is equipped with the fiber optic downwelling irradiance sensor (FODIS) for VNIR data.

Laser Scanner

The laser scanner is a latest generation LiDAR sensor, during the campaign the model Riegl LMSQ560 has been used, it allows the Full Waveform Analysis; and is able to record the Full Waveform by storing all the target echoes, instead of 2 (first and last echoes) or 4 discrete echoes usually collected by the most common laser altimeters. It is worth nothing that the "Full waveform" mode, thanks to the ability to record the whole multiple echoeKLs waveform, assures the penetration of even the thick vegetation so as to obtain accurate DTMs in the presence of canopy. This laser scanner is equipped by a polygonal rotating mirror which sends signals to the ground with a frequency settable up to 240.000 Hz, with a maximum scanning angle of 60 degrees and a beam divergence of 0.5 mrad. It is important to point out that the system does not pose any risks to human health since it falls into the Eye Safety Class 1, which makes the instrument usable in many application fields and in many different locations. The laser beam is sent to the ground with a specific frequency in the near-infrared band and the echoes are stored and 16-bit sampled (Table 6).

HYPER-SPECTRAL SYSTEM		
	VNIR	SWIR
Imaging Spectrometer	ImSpector V10E (Specim)	ImSpector N25E (Specim)
Spectral Range	400-1000 nm	1000-2500 nm
Spectral Resolution	2.8 nm	10 nm
Spectral Sampling	1.2 nm	6.3 nm
Spectral bands	504	239
Spatial pixels	1024	320
Focal length	9 mm	15 mm
Digital resolution	12 bit	14 bit
FOV	± 34.32°	± 18.00°

Table 5 Technical characteristics of the hyper-spectral system.
Tabella 5 Caratteristiche tecniche del sistema iperspettrale.

LASER CHARACTERISTICS	
Wavelength	1550 nm
Pulse length	3.5 ns
Beam divergence	0.5 mrad
Type/class laser	Class 1
Eyesafe range	0 m
ACQUISITION METHODOLOGY	
Scanning Method	Polygonal rotating mirror
Mirror rotation speed	5 - 160 KHz
Pulse Frequency	40 - 240 KHz
Maximum scanning angle	60°deg
Maximum Number of echoes/pulses recorded	unlimited
Digitizer sampling Frequency	1 GHz
Measurement	Full Waveform
Signal intensity dynamic Range	16 bit
PRECISION AND RESOLUTION	
Precision range (2 sigma)	2 cm
Precision elevation (2 sigma)	6 cm @ 1,000 m AGL
Overall planimetric precision (2 sigma)	0.30 cm @ 1,000 m AGL
Max. # points/m^2	156 points @ 50 m AGL, 30 Kts

Table 6 Technical characteristics of the Laser Scanner.
Tabella 6 Caratteristiche tecniche del Laser Scanner.

THERMAL CAMERA	
Brand	DigiTHERM
Sensor	Uncooled microbolometer
Beam divergence	0.5 mrad
Pixel thermal image	640 (H) x 480 (V) pixel
Spectral range	7.5 - 14 µm
Standard temperature range	-40° - +120°C
Thermal resolution of NETD	< 50mK
Measurement accuracy	±1.5 K otherwise ± 2 K
Operating temperature	-15 - +50°C
Relative humidity	10% to 95%, non-condensing

Table 7 Technical characteristics of the Thermal Camera.
Tabella 7 Caratteristiche tecniche della Camera Termica.

Thermal camera

The digital thermal camera is the DigiTHERM for digital aerial thermography. It's a uncooled microbolomer FPA-detector that delivers thermal images of 640x480 pixels. With a thermal resolution of 0.05K the standard temperature range is -40°C to 120°C (Table 7).

Digital Camera

The Digital Camera is the DigiCAM with a lens of 50mm, that enables acquisition of digital aerial photography. Among the main characteristics it is worth mentioning the high resolution (39 Megapixel), the possibility to record frames in the Color-Visible (VIS) or in the Color-Infrared (CIR), with the use of special filters (Table 8).

4. Satellite data Acquisitions

The Etna 2012 campaign has been organized taking into account the 2 scheduled reference satellite acquisitions: TERRA ASTER and EO1-HYPERION. Both satellite data will be used to improve the simulation of PRISMA data based on the airborne multi-sensor platform acquired data. The reference satellite acquisition have been requested at NASA JPL ASTER group and at Goddard Space Flight Center. They are shown in Table 9.
Respect to the scheduling shown in Table 8, TERRA-ASTER daytime image of June 25 and EO1 HYPERION images of June 23, 26 and 28 have been acquired (Figure 15). Only the image acquired on June 26 is cloud free. All the images have been released by providers.

DIGITAL CAMERA	
Brand	DigiCAM
Resolution	39 Mpixel
CCD sensor dimension	36.80 x 49.07 mm
Pixel size	6.8 µm
Filter array	Interchangeable Color (RGB) or Color Infrared (CIR)
Lens	50 mm
Image data format	TIFF, JPEG, DNG (Optional 8 or 16 bit)

Table 8 Technical characteristics of the Digital Camera.
Tabella 8 Caratteristiche tecniche della Camera Digitale.

Satellite/sensor	DAY TIME
TERRA/ASTER	25/06/2012 9:45 GMT
EO1 HYPERION	2012-06-23T09:14:00Z prioritaire
	2012-06-26T09:28:00Z prioritaire
	2012-06-28T09:05:00Z prioritaire
	2012-07-01T09:19:00Z
	2012-07-06T09:11:00Z

Table 9 Scheduling of satellite/sensor acquisition.
Tabella 9 Pianificazioni delle acquisizioni da satellite.

4.1 ASTER

The satellite platform TERRA launched by NASA as part of the EOS (Earth Observing System) is equipped with ASTER (Advanced Spaceborne Thermal Emission and Reflection Radiometer), an instrument developed by a cooperation of NASA, the Japan's Ministry of Economy, Trade and Industry, and ERSDAC (Earth Remote Sensing Data Analysis Center).

ASTER is constituted by three different subsystems, operating in the visible and near infrared (VNIR), short wave infrared (SWIR) and thermal infrared (TIR) regions of the electromagnetic spectrum. Each subsystem is provided with a different telescope. The main instrument characteristics are summarized in Table 10, ASTER data are collected upon request on specific scenes.

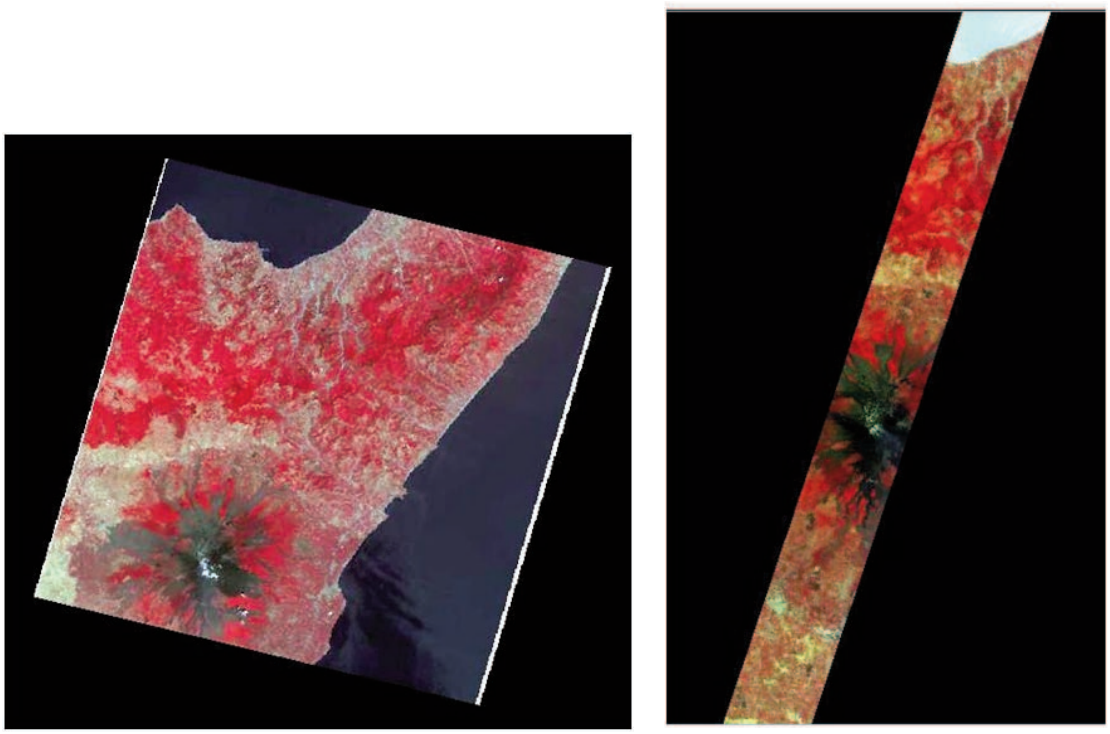

Figure 15 TERRA-ASTER image (left) acquired on June 26, 2012; and EO1-Hyperion image (right) acquired on June 28, 2012.
Figura 15 Immagine TERRA-ASTER (a sinistra) acquisita il 26 giugno 2012 e immagine EO1-Hyperion (a destra) acquisita il 28 giugno 2012.

Characteristic	VNIR	SWIR	TIR
Spectral Range	Band 1: 0.52-0.60 µm Nadir looking	Band 4: 1.600-1.700 µm	Band 10: 8.125-8.475 µm
	Band 2: 0.63-0.69 µm Nadir looking	Band 5: 2.145-2.185 µm	Band 11: 8.475-8.825 µm
	Band 3: 0.76-0.86 µm Nadir looking	Band 6: 2.185-2.225 µm	Band 12: 8.925-9.275 µm
	Band 4: 0.76-0.86 µm Backward looking	Band 7: 2.235-2.285 µm	Band 13: 10.25-10.95 µm
		Band 8: 2.295-2365 µm	Band 14: 10.95-11.65 µm
		Band 9: 2.360-2.430 µm	
Ground Resolution	15 m	30 m	90 m
Data Rate(Mbit/s)	62	23	4.2
Cross-track Pointing (deg)	±24	±8.55	±8.55
Cross-track Pointing (Km)	±318	±116	±116
Swath Width (Km)	60	60	60
Detector Type	Si	PtSi-Si	HgCdTe
Quantization (bits)	8	8	12

Table 10 ASTER characteristics.
Tabella 10 Caratteristiche del sensore ASTER.

4.2 Hyperion

During the field measurements campaign Hyperion acquisitions have been requested in the frame of a collaboration between INGV, USGS and NASA. Hyperion is an imaging sensor on board of the Earth Observing (EO-1) platform. The EO-1 satellite was launched on 21th November 2000, and is positioned in a polar orbit at 705 Km of altitude with a 16-day repeat cycle. The orbit is slightly to the east of Landsat-7 passing over the same ground-track one minute later. EO-1 joins a 'morning constellation' of Earth observing satellites, including SAC-C and Terra, all examining electromagnetic radiation along the same ground track with different swath widths and with a range of spatial and spectral resolution.

The three primary instruments on board are Hyperion, ALI (Advanced Land Imager) and Leisa-AC (Linear Etalon Imaging Spectrometer Array–Atmospheric Corrector). ALI is similar to Landsat 7 with ten spectral bands with a spatial resolution of 30 m for the multispectral bands and 10 m for the panchromatic band.

The Hyperion is the first space hyperspectral imaging spectrometer. It collects 220 unique spectral channels ranging from 0.357 to 2.576 mm with a 10 nm bandwidth. The instrument operates in a pushbroom mode, with a spatial resolution of 30 m for all bands. The standard scene width is 7.7 km. Standard scene length is 42 km, with an optional increased scene length of 185 km. In the period

Parameters	ALI	Hyperion
Spectral Range	0.4-2.4 µm	0.4-2.4 µm
Spatial Resolution	30 m	30 m
Swath Width	36 Km	7.6 Km
Spectral Resolution	Variable	10 nm
Spectral Coverage	Discrete	Continuous
Pan Band Resolution	10 m	N/A
Total N° of Bands	10	220

Table 11 Hyperion main sensor parameters.
Tabella 11 Principali parametri del sensore Hyperion.

17-26 July Hyperion acquired data on the 19th in the nadir view and on the 26th with an inclination angle of about 8 degrees. In Table 11 sensors characteristics are reported.

5. Field measurements campaign

During the field campaign the surface characteristics of Etnean area have been analyzed in order to validate the satellite data acquired in the time window of the campaign. As already mentioned before, 3 test sites were selected in etnean area: Mount Etna, Ciclopi islands and Paternò "Salinelle" area. The description of Mt Etna site is reported in Annex A. During the 25/06/2012 aerial acquisition above Ciclopi islands, field Hyperspectral (Spectroradiometer) and Temperature measurements have been performed using a Spectroradiometer Fieldspec Pro and a Thermal Camera. The Fieldspec Pro has allowed to acquire radiance spectra of the marine surface that shows a spectral behaving that can be approximated to a black body. At the same time measure of brightness temperature have been performed on the same surface using the Thermal Camera. The obtained integrated dataset allows to validate the Remote Sensing data by comparing the PRISMA spectra to the Fieldspec data calibrated with brightness temperatures. Different instruments have been used during the campaign:

- a spectroradiometer Fieldspec Pro to measure the surface reflectance of various volcanic products present in the area;
- a Laser scanning for the surface characterization of volcanic outcrops;
- gps, thermal camera, a photometer and a "unilogger" to evaluate the atmospheric and thermal characteristics of measure sites;
- a FTIR (Fourier Spectrometer) used to measure the surface emissivity of outcropping materials.

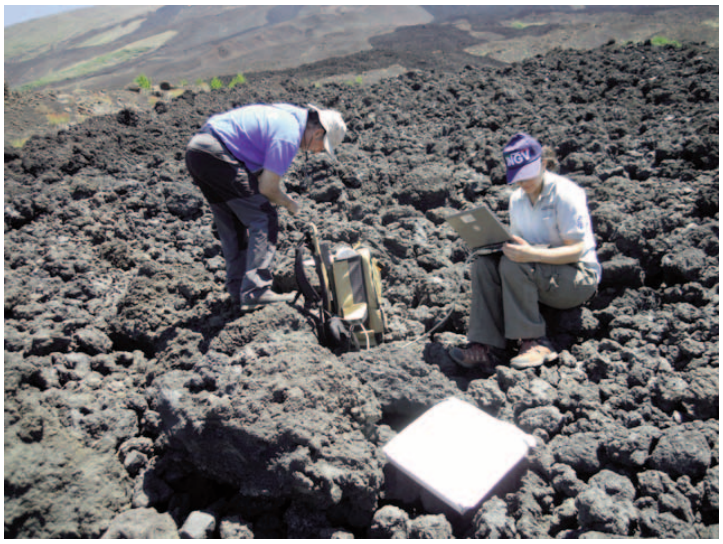

Figure 16 FieldSpec acquisition on 1999 basaltic lava flow.
Figura 16 Acquisizione con il FieldSpec su una colata lavica del 1999.

5.1 Surface Reflectance Spectroscopy

Measurements of solar reflected radiance were carried out with a FieldSpec FR portable spectroradiometer (Analytical Spectral Devices, Inc., 1994). Three separate spectrometers covers the 350-2500 nm spectral range. The first one operates between 350 and 1000 nm, with a spectral resolution (FWHM) of approximately 3 nm and a sampling step of 1.4 nm; the other two cover the region from 900 to 1850 nm and 1700 to 2500 nm respectively. The sampling in these regions is every 2 nm and the resolution varies between 10 and 11 nm. The instrument uses a trifurcated fiber-optic cable to sample the light field being measured. Measurements were made directly with the fiber-optic cable, that has a field of view of 25°. Data storage, visualization and calibration are performed in real time by a dedicated software on a personal computer connected to the instrument (Figure 16).
Two FieldSpec FR portable radiometers were used to measure the surface reflectance spectra. Selected test sites have been chosen in order to complete the Spectral Data-base of Mt. Etna surface rocks. The yellow dots in the geological map of Mt Etna indicate the site locations where spectra of targets have been acquired (Figure 17).

5.1.1 Measured sites

Site locations were determined by GPS. In Annex B the table containing the sites location and the targets sampled is reported.

5.1.2 Surface materials spectra

In Figure 18, Figure 19, Figure 20 and Figure 21, four targets and their spectra are shown: first target is blocks of 1852-1853 lava covered by lichens and tephra at Milo site location; second target is the 2002 basaltic lava flow at Forest Reserve road site location; third target is lava covered by tephra and brush at Strada forestale site location; fourth target is a Mud at Paternò site location.
The noisy wavelength range of spectra correspond to the water vapor absorption bands. The atmospheric water vapor affect the acquired spectra in the following wavelength ranges: 1370-1413 nm, 1812-1933 nm and after 2300 nm.

5.2 Ground based topography acquisition

The local morphologies of volcanic surfaces at selected sites (Figure 22) have been reconstructed at sub-meter scale with two different techniques: i) 3D scansion of the surface by a terrestrial Laser scanner device [Mazzarini et al., 2008], ii) 3D

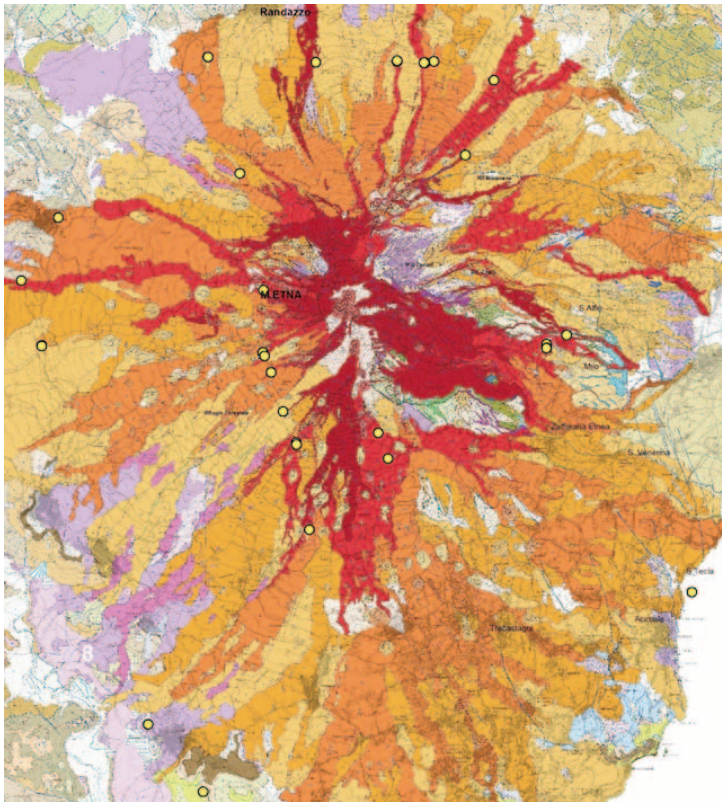

Figure 17 Map of Fieldspec Pro measurements locations.
Figura 17 Mappa dei siti di misura del Fieldspec Pro.

reconstruction based on sequences of images taken with digital cameras [Favalli et al., 2012].
Eight sites have been surveyed, six are lava surfaces ranging in age from late Holocene to the 1999 eruption blanketed with pyroclastic deposits formed during the explosive eruption in the last ten years. The other two sites are in the south-western slope of the volcano, close to the town of Paternò, in the Salinelle area (active mud volcanoes). In Table 12 the type of surface and the associated topographic surveys are reported.

5.2.1 Ground based 3D laser scanning

3D scansion of the surfaces have been acquired by using a Konica Minolta VI-910, which is a remote non-contact 3D digitizer (www.konicaminolta-3d.com), to derive through Laser triangulation x, y and z coordinates of imaged objects. The objects are scanned by a plane of laser light emitted from the VI-910's source aperture. The Laser light (690 nm) is reflected from the surface of the scanned object and registered by the instrument. Each scan line is observed by a single frame and captured by a CCD camera. The surface shape is converted to a grid of over 300,000 vertices (connected points). The VI-910 is provided with three interchangeable lenses that can accommodate measurement of objects of various sizes and distances from the lens. A single scan is capable of capturing an angular field of view of approximately 10 cm^2 (TELE lens) to 0.8 m^2 (WIDE lens). The scansion has an accuracy of 0.22 mm in x, 0.16 mm in y and 0.1 mm in z axis for the TELE lens with 300,000 vertices. The WIDE lens accuracy is 1.4 mm along x, 1.04 mm along y and 0.4 mm along z; the z axis is the optical axis of the laser scanner.
During measurements, the laser is mounted on a tripod and positioned at nadir with respect to the surface. In such a way, the z values are the elevation of the surfaces. The surfaces sampled at Mt. Etna have areas up to 1 m^2 and have been imaged at a distance of about 1 m.

3D reconstruction from photos

The 3D reconstruction from photos (Figure 23) is achieved using the open source code Bundler, which can process from a minimum of 4-5 up to several hundreds of images (Snavely et al., 2007). It is a 'Structure from Motion' code, which allows to remove the camera distortion, to calculate the camera shooting position and orientation, and to obtain a preliminary 3D reconstruction of the surface as a reduced point cloud (key points). A more complete and accurate reconstruction is carried out starting from the key points with the open-source Patch-based Multi-View Stereo code (Furukawa and Ponce, 2009) that, in this case, allows the reconstruction of surfaces with meters scales with model errors less than 1 cm [Favalli et al., 2012].

L3D	P3D	Surface type
	X	Lava flow 1999
X	X	Lava flow Holocene
X	X	Lava flow 1787
X	X	Lava flow 1780
X	X	Lava flow 1852-53
X	X	Lava flow 1971
X	X	Mud volcano
X	X	Mud volcano

Table 12 Topographic surveyed surfaces; L3D: 3D laser scanning; P3D: 3D reconstruction from photos.
Tabella 12 Superfici rilevate topograficamente; L3D: laser scanning 3D; P3D: ricostruzione 3D dalle foto.

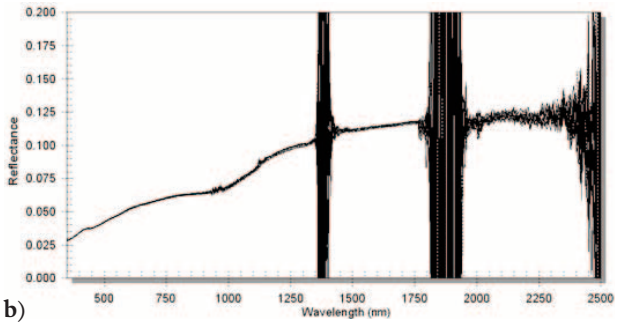

b)

Figure 18 a) Picture of blocks of 1852-1853 lava covered by lichens and tephra target at Milo site location; b) target spectrum.
Figura 18 a) Foto di blocchi di lava del 1852-1853 coperti da licheni e tephra a Milo; b) spettro del target.

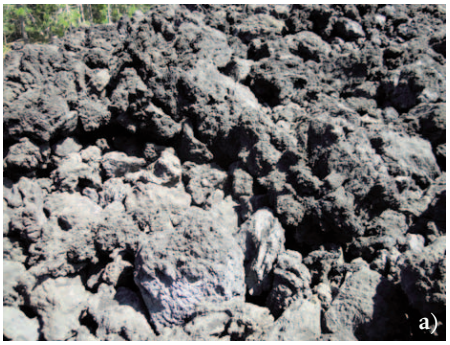

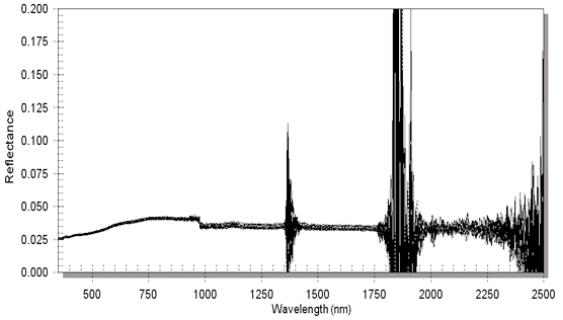

b)

Figure 19 a) Picture of Lava 2002 blocks target at Strada forestale site location; b) target spectrum.
Figura 19 a) Foto di blocchi di lava del 2002nel sito della strada Forestale; b) spettro del target.

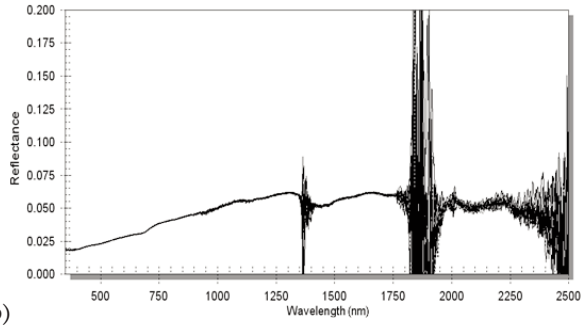

b)

Figure 20 a) Picture of mix tephra, lava and bush target at Strada forestale site location; b) target spectrum.
Figura 20 a) Foto di tephra, lava ed essenze arboree nel sito della Strada Forestale; b) spettro del target.

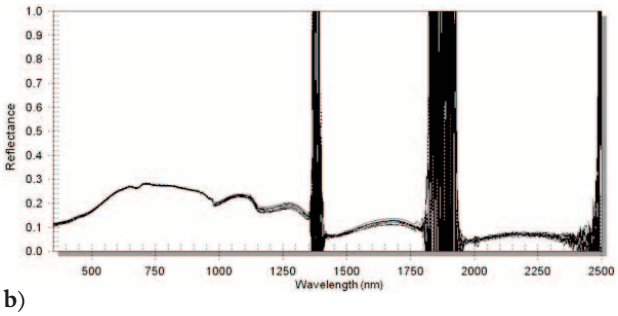

b)

Figure 21 a) Picture of mud target at Paternò site location; b) target spectrum.
Figura 21 a) Foto del fango al sito di misura di Paternò; b) spettro del target.

Roughness computation

In order to qualitatively describe the surface roughness, the Root Mean Square of Heights (σ) and the Allan Deviation (v) have been computed [Mazzarini et al., 2008].
The Root Mean Square of Heights (σ) is defined as:

$$\sigma = \left\{ \frac{1}{n-1} \sum_{i=1}^{n} \left[z(x_i) - \bar{z} \right]^2 \right\}^{1/2} \quad (1)$$

where $z(x_i)$ is the elevation of point in position x_i, the average elevation and n is the number of points. The σ has been computed over the whole area, the surfaces have been detrended [Shepard et al., 2001] by subtracting the best-fit plane. The lower the σ, the smoother the surface.
The Allan Deviation or Root Mean Square deviation (v) is function of the Δx lag, and it is defined as:

$$v(\Delta x) = \left\{ \frac{1}{n} \sum_{i=1}^{n} \left[z(x_i) - z(x_i + \Delta x) \right]^2 \right\}^{1/2} \quad (2)$$

where $z(x_i)$ is the elevation of point of position x_i, n is the number of points, and Δx is the lag used. The function $v(\Delta x)$ is computed averaging both horizontal and vertical de-trended profiles derived from 3D Laser scansion.
Topography of natural surfaces is assumed to be self-affine such that increasing the scale of the x and y axes by a factor r must be compensated for in the z direction by a factor r^H, where H is the Hurst exponent ($0 < H < 1$). Visually, surfaces with $H > 0.5$ look smoother than surfaces with $H < 0.5$ [Mazzarini et al., 2008 and references therein]. The Hurst exponent is related to the commonly used fractal dimension D, by $D = 2 - H$ in the case of a profile and $D = 3 - H$, for a surface.
For an ideal fractal, the conventional parameters σ and v, among other, change with scale, while H is strictly the same. In order to derive H, we start by computing v, as in (2), for different values of the step size Δx. If topography is indeed self-affine, equation (3) holds:

$$v(\Delta x) = C \times \Delta x^H \quad (3)$$

where C is a constant.

Figure 22 Locations of the measured sites.
Figura 22 Siti di misura.

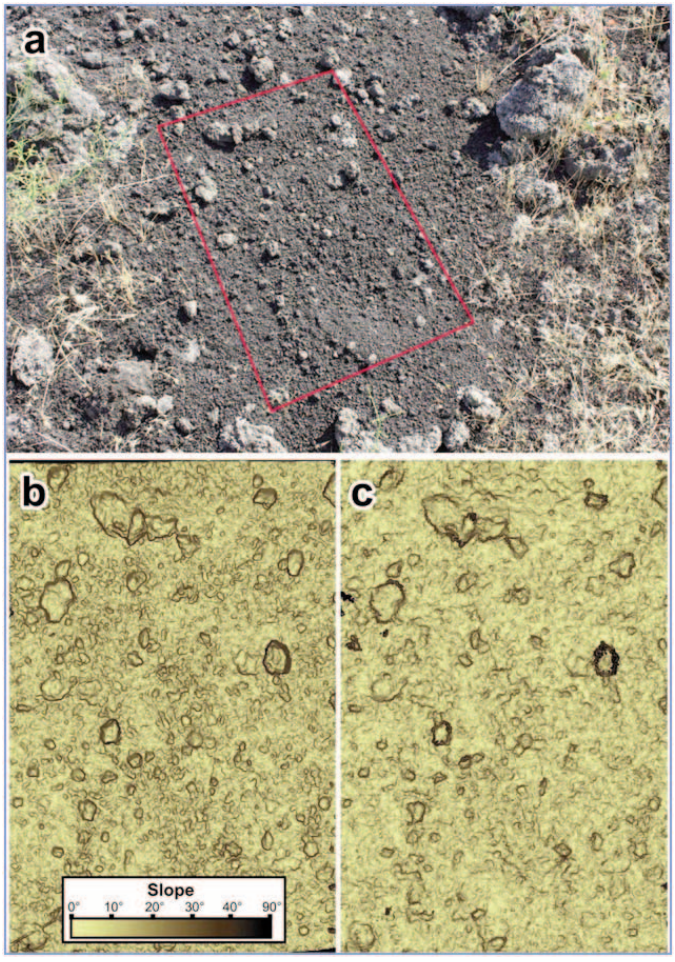

Figure 23 Topography reconstruction of the site on the 1852-1853 lava flow between the villages of Milo and Fornazzo. a) Photo of the sampled area (0.25 m^2, red polygon). b) Slope image of the digital model acquired with the Konica Minolta VI-910 3D digitizer. c) Slope model of the digital model reconstructed with a "Structure from Motion" technique from a set of 41 shots.
Figura 23 Ricostruzione topografica del target sulla colata lavica del 1852-1853 tra i paesi di Milo e Fornazzo. a) foto dell'area campionata (0.25 m^2, poligono rosso). b) immagine della pendenza del modello digitale acquisito tramite un digitalizzatore Konica Minolta VI-910 3D. c) modello di pendenza del modello digitale ricostruito con una tecnica "Structure from Motion" da una serie di 41 scatti.

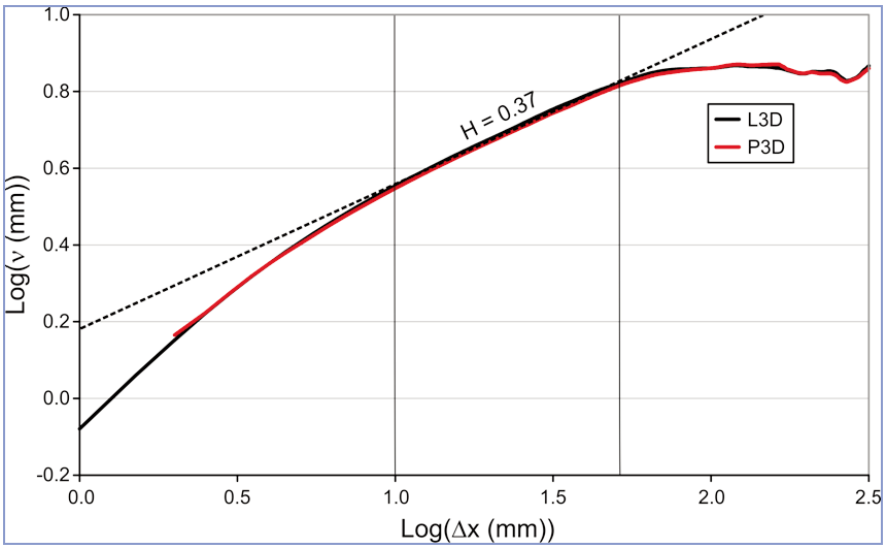

Figure 24 Allan deviation (v) vs. length (Δx) is drawn in a log-log plot for the 1852-1853 lava flow surface. The slope of the curves defines the Hurst exponent (H). The best fit linear line is outlined and the relative H value is reported. Vertical black lines mark the range where the linear fit is computed.
Figura 24 Deviazione di Allan (v) vs lunghezza (Δx) vengono rappresentate in un grafico log-log relativo alla superficie della colata lavica 1852-1853. La pendenza delle curve definisce l'esponente di Hurst (H). Il miglior fitting lineare è evidenziato ed il relative valore di H è riportato. Le linee nere verticali definiscono il range entro il quale è calcolato il fitting lineare.

Thus, H is derived as the slope of the best fit line of log $v(\Delta x)$ vs. log Δx. The computation of H is done in the length range where the curve exhibits a linear trend.
For example, the roughness of surface sampled in the 1852-1853 lava flow has been computed according to equations (2) and (3). In Figure 24 the log-log plots of Allan deviation vs Length is displayed for both laser 3D and photo 3D reconstructions, giving an Hurst exponent of 0.38 in the range 1 – 50 mm for both methods. Applying equation (1) the roughness of the sampled surface is 12.7 mm for laser 3D and 12.4 mm for the photo 3D reconstructions respectively.

5.3 Surface Temperature

During this measurements campaign a Thermoteknix System Ldt VisIR 640 thermal camera has been used to collect thermal images over different areas. The instrument is kept in a rugged industrial housing including a central optics pod for different orientation image acquisition. The camera work in 8-14μm spectral range and has an articulated central optics pod for different orientation image acquisition. Measurements have been collected by using a default set up which is able to set, automatically, the suitable dynamic range defining the hotter and colder spot of the sensed image. During the Etna campaign it has been used both by hand and on a tripod. Tripod has been preferred in the long term acquisitions of 25th June 2012 on Pian del Lago site (Figure 25) where images were collected every 10 seconds for 15 minutes.

Figure 25 Thermal camera mounted on tripod.
Figura 25 Camera termica montata sul treppiede.

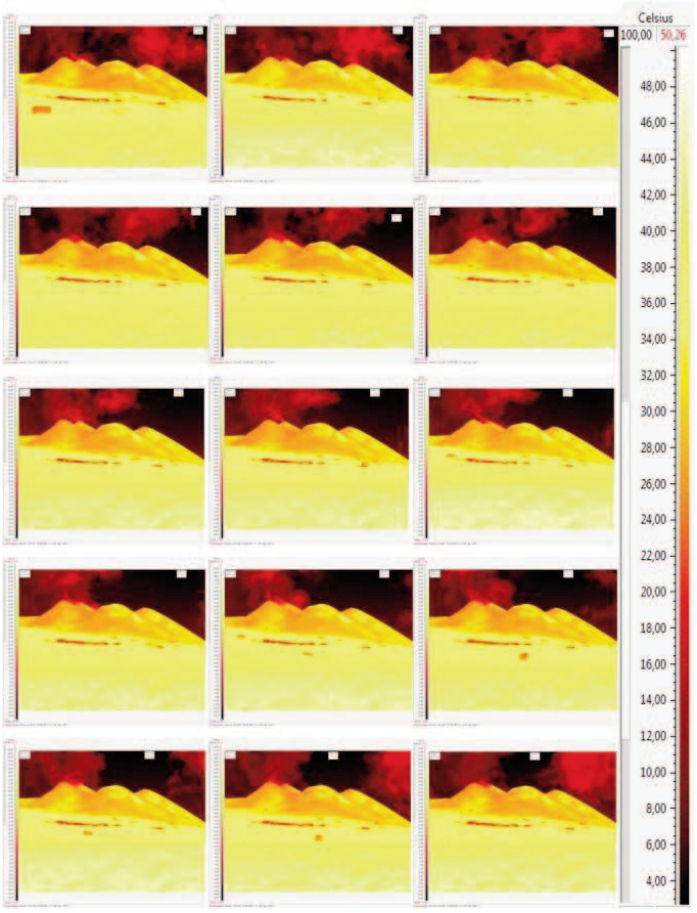

Figure 26 Time sequence of thermal camera acquisitions of Etna SE crater. The scale bar shows the temperature in degrees Celsius in a scale ranging from 16 to 64°C.
Figura 26 Sequenza temporale di acquisizioni del cratere di SE dell'Etna. La scala riportata in ogni immagine mostra la temperatura in gradi centigradi nell'intervallo tra 16 e 64°C.

5.3.1 Collected Data

Before the campaign the thermal camera was tested in a laboratory in order to set the temperatures range expected during the field acquisitions. Thermal images were collected on 25th June 2012 from 9.40 AM local time up to 12.26 AM local time. The timetable was scheduled according to the ASTER pass time over Mt. Etna summit. Figure 26 shows a subset of the 118 images collected at Pian del Lago.

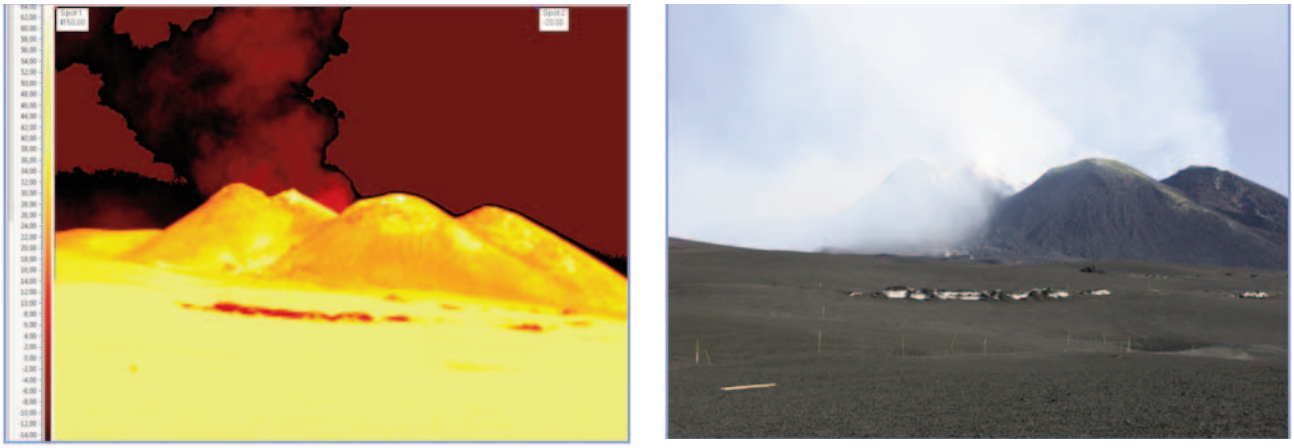

Figure 27 Thermal image (left) and visible image (right) taken from Pian del Lago (37°44'12.49"N 15°00'24,17") toward Etna SE crater.
Figura 27 Immagine termica (sinistra) ed immagine nel visibile (destra) ripresa da Pian del Lago (37°44'12.49"N 15°00'24,17") verso il cratere di SE dell'Etna.

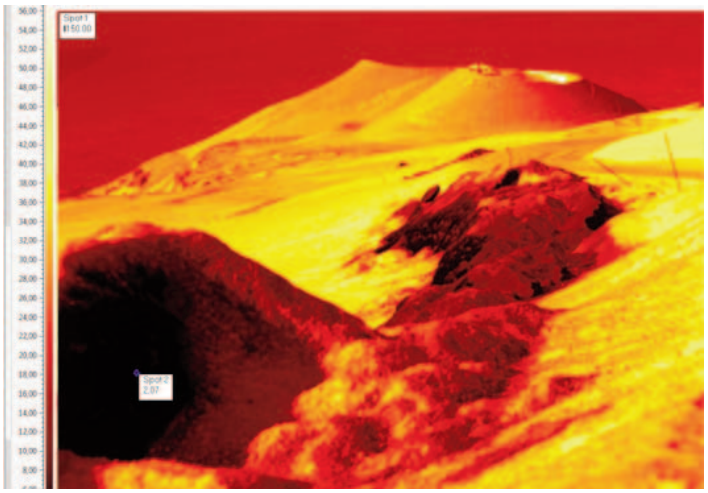

Figure 28 Thermal image of the area acquired from Cisternazze crater (37° 44' 12.49"N 15° 00' 24,17") toward south. The temperatures are in degree Celsius and range from 6 to 56°C.
Figura 28 Immagine termica dell'area ripresa dal cratere di Cisternazze (37°44'12.49"N, 15°00'24,17") verso Sud. Le temperature sono espresse in gradi Celsius nell'intervallo da 6 a 56°C.

Thermal images were acquired starting from the SE crater and moving southward. The following Figure 27 and Figure 28 show the thermal and visible images acquired few hundreds of meters far away the starting point close to the SE crater.

5.4 Emissivity measurements

FTIR measurements have been planned as complementary field characterization. FTIR instruments best operation time is usually from sunrise to few hours later and from sunset to few hours later.
Although the acquisition time has not been optimal for emissivity measurements, a data set has been acquired by using two different instruments: a micro FTIR and a Bruker operating in the same spectral range but with a different spectral resolution.

5.4.1 FTIR spectrometer description

The first instrument used is the MicroFTIR, Model 102F spectrometer (Figure 29), developed by Design and Prototypes LTD for field measurements of Earth's surface and atmosphere spectral radiance. The spectrometer operates at wavelengths ranging from 2 to 16 mm with a spectral resolution of 2 cm^{1}. In Table 13 its characteristics are shown. Two HgCdTe (or MCT) and InSb liquid nitrogen cooled detectors allow measurements collection in the 8-14 mm and 3-5mm atmospheric windows respectively.
A second portable FTIR instrument for emissivity measurements has been used during the campaign, it is a OPAG-22 FTIR (Bruker Daltonics, Germany). The FTIR Bruker spectrometer collects spectra at up to 0.5 cm^{-1} resolution, using a ZnSe beamsplitter and LN_2 cooled MCT detector, in a wavenumber range from 500 to 6000 cm^{-1}. The instrument field of view is 30 mrad. The instrument weights 19 kg and has dimensions of 37x40x26 cm.

5.4.2 Description of the emissivity measurements

The measurements have been executed in different test sites: Torre del Filosofo, Paternò mud volcano and some types of Etna lava flows. Table 14 summarizes the measurements sites and targets while the acquired samples and their related spectra are shown in figures 30-34; the spectral range 7-8 μm is quite noisy because most of the emissivity measurements

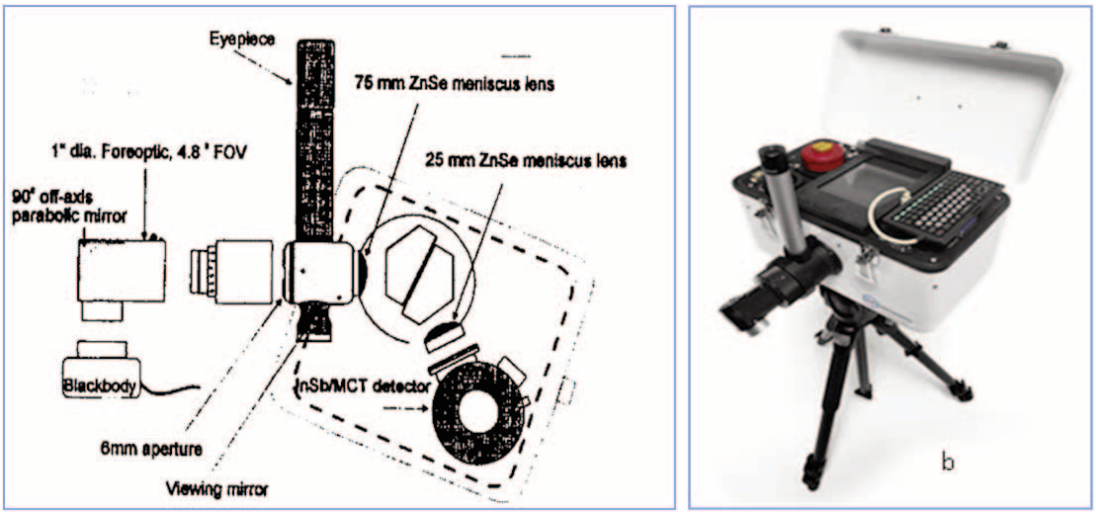

Figure 29 Schematic diagram of the model 102F portable FTIR by Design & Prototypes,LTD (left) and the snapshot of the instrument (right).
Figura 29 Diagramma schematico dell'FTIR portatile 102F della Design & Prototypes LTD (sinistra) e foto dello strumento (destra).

have been executed late in the morning when the environmental temperature was about 35°C.

Spectral Range	2-16 µm
Spectral Resolution	2 cm^{-1}
Operating temperature range	15-35 °C (instrument temperature)
FOV	4.8° (additional input optic 2.4°)
Computer OS and type	DOS 6.22, 8GB HD, Pentium 166MHz/32MB
Input voltage range	12V DC (±10%)
Weight	7 Kg
Size	36cmx20cmx23cm

Table 13 Main features of the model 102F portable FTIR by Design & Prototypes, LTD.
Tabella 13 Principali caratteristiche del FTIR portatile 102F di Design & Prototypes, LTD.

In the following figures emissivity measurements are shown as collected during the field campaign in the spectral range 7-14 µm. Only the spectrum acquired in Paternò site has been smoothed to reduce the noise and the spectral range has been shortened to the atmospheric window 9-10 µm (Figure 31).

5.5.1 CO_2 flux measurements

Soil gas surveys were focused on the determination of diffuse CO_2 efflux from the ground. Water temperature was also measured in the muddy pools of the Salinelle of Paternò. Diffuse CO_2 efflux measurements were carried out in a site located on the lower south-west flank of the volcano at an elevation of 421 m asl, about 2 km SE of the town of Paternò and 2.6 km south of the Salinelle mofete.
Diffuse CO_2 emissions were measured using the accumulation chamber method (Figure 35), which consists of measuring the rate of increase of the CO_2 concentration inside a cylindrical chamber opened at its bottom placed on the ground surface. The chamber is provided with an internal fan to achieve an efficient gas mixing and is connected with a portable NDIR (nondispersive infrared) spectrophotometer (PP Systems, UK, mod. EGM4). The accumulation chamber is placed firmly on the ground surface so as to avoid intrusion of air inside of it. Before being pumped to the spectrophotometer, the gas is filtered in order to trap any eventual water vapour, whose presence can create analytical interferences and can also damage the IR cell in case of vapour condensation. The gas inside the chamber is constantly pumped from the chamber to the IR spectrophotometer and then sent again into the chamber. The change in concentration during the initial measurement is proportional to the efflux of CO_2 [Parkinson, 1981; Tonani and Miele, 1991; Chiodini et al., 1998]. This is an absolute method that does not require corrections linked to the physical characteristics of the soil. We tested the method in the laboratory with a series of replicate measurements of known CO_2 effluxes. The average error was about ±5%, which is assumed as a random error in the natural emission rates. The reproducibility in the range 200 – 1600 g m^{-2} d^{-1} was 5%. The average efflux value measured at the site near Paternò on 15th

Date	Day Time	Measurement sites	Target	Instrument and Notes
25.06.2012	Afternoon	Torre del Filosofo	Tephra sample (Fig.30)	Micro FTIR Strong wind and environmental temperature about 35°C
26.06 2012	Morning	Paternò "Salinelle"	Mud and bubbling water pool (Fig.31)	Micro FTIR
	Morning	Monti Silvestri	1892 lava: basaltic block (Fig.32) Surface materials (Fig.33)	FTIR Bruker
	Morning	Monti Silvestri	Lava 1991 (Fig 34)	FTIR Bruker

Table 14 Emissivity measurements sites.
Tabella 14 Siti di misura di emissività

5.5 Gas Emission

Gas emissions from both the summit and the flanks of Mount Etna volcano have been monitored using Remote Sensing techniques and on-site monitoring devices. In particular the CO_2 rich soil degassing and variations in SO_2 flux have been analyzed during the campaign.

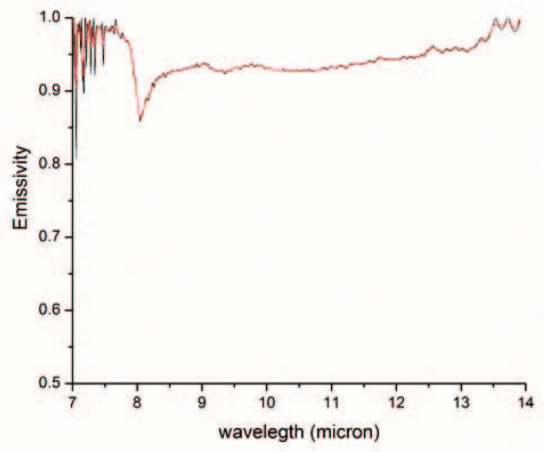

Figure 30 Torre del Filosofo sample.
Figura 30 Campione dal sito di Torre del Filosofo.

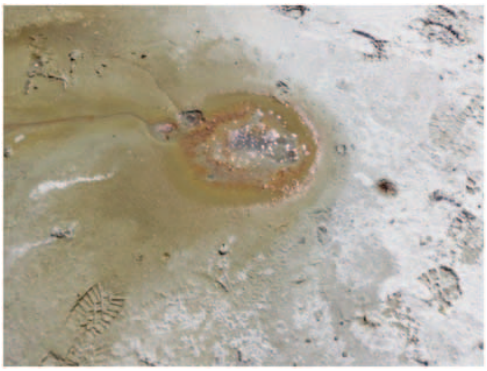

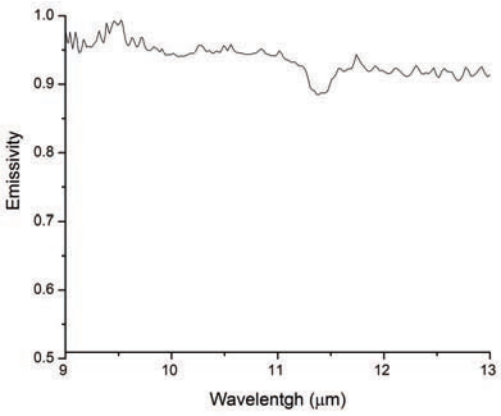

Figure 31 Le Salinelle Mofete.
Figura 31 Sito delle Salinelle.

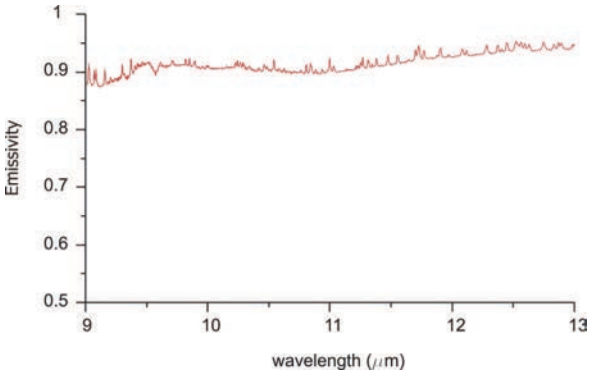

Figure 32 Basaltic rock (1892 lava).
Figura 32 Roccia basaltica (lava 1892).

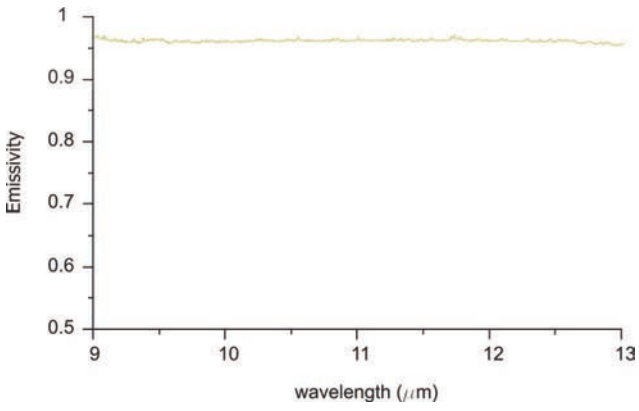

Figure 33 Surface materials of Serra Pizzuta.
Figura 33 Materiali superficiali di Serra Pizzuta.

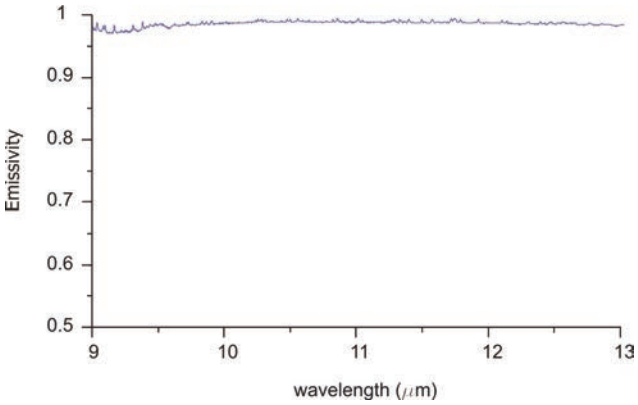

Figure 34 1991 lava.
Figura 34 Lava del 1991.

June, 2012 was 1973 g m^{-2} d^{-1}, and that measured on the 2nd of July, 2012 was 2031 g m^{-2} d^{-1}. These values are part of a period characterized by a general increasing trend of diffuse degassing in this sector of the volcano (Figure 36) that culminated in early October 2012, probably as a consequence of the development of volcanic activity at Mt. Etna.Water temperature measurements were carried out using a non-contact laser-guided IR temperature meter (Fluke Corporation, WA, US, mod. Fluke 68), with accuracy of ±1% for targets above 23 °C and of ±2 °C for targets between -18 °C and 23 °C. The highest temperature measured on 27th of June, 2012 in the water and mud issuing from the Salinelle mofete at Paternò was 22 °C, in agreement with previous and following measurements carried out during 2012 (maximum temperature values ranged between 20 and 28 °C). This was a rather low value (the highest temperature measured at this site in the past 150 years was almost 50 °C, Silvestri, 1866, 1878) that indicates a stable degassing activity at this site during the PRISMA campaign.

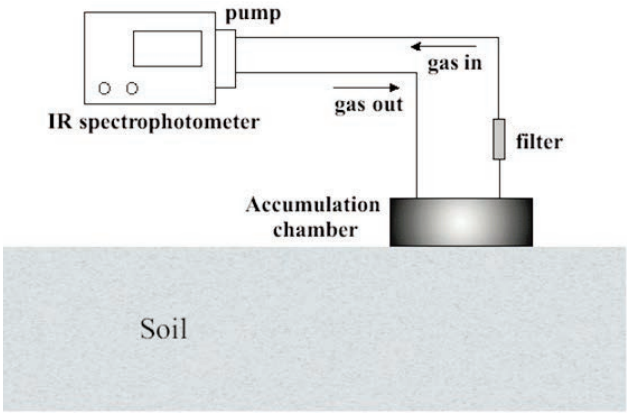

Figure 35 Sketch of the system used for measuring soil CO_2 fluxes.
Figura 35 Schema del sistema utilizzato per misurare il flusso di CO_2.

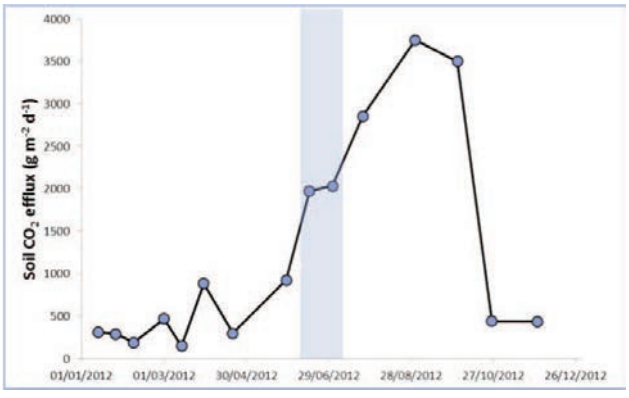

Figure 36 Soil CO2 fluxes.
Figura 36 Flusso di CO2 del suolo.

5.5.2 SO_2 flux measurements

We report bulk SO_2 flux from Mt Etna's summit craters collected on 25 June 2012 by means of the FLAME network (Flux Automatic MEasurement, Figure 37). The network consists of nine autonomous ultraviolet scanning spectrometer station (UV-Scanner) installed at an altitude of ~900 m asl on the flanks of Mt Etna and spaced ~7 Km apart [Salerno et al., 2009b; Campion et al., 2009]. Each UV-Scanner station consists of an Ocean Optics S2000 spectrometer coupled with an ADC1000-USB A/D analogue -to-digital converter. The spectrometers is connected via fibre optics (1000 m) to a two-quartz-lens telescope (8 mrad Field of View) mounted in a rotating head that allows a scanning of the sky above the station for ~150°. A coated visible-light filter (Hoya U330) is installed as a window in the rotating head to reduce stray light inside the spectrometer and for environmental protection. The light exposure of the detector is automatically adjusted throughout the day to optimize the signal. The device is controlled by a micro-controller mounted on a custom-made circuit board [Caltabiano et al., 2005]. Each station scans the sky for almost 9 h, intersecting the plume at a distance of ~14 km from the volcano summit craters and acquiring a complete scan in ~5 min. SO_2 col-

Satellite (Sensor)	Time of passage of Satellite (hh:mm, GMT)	SO_2 flux (a^{-1}) and recording time (hh:mm, GMT)
TERRA / ASTER	09:54	1231 ; 09:52 1498 ; 09:56
EO-1 / HYPRION	10:00	743 ; 10:00

Table 15 Time of passage of ASTER and Hyperion satellites and SO_2 flux values obtained by FLAME network.
Tabella 15 Passaggi dei satellite ASTER e Hyperion e valori di flusso di SO_2 ottenuti dalla rete FLAME.

Figure 37 Map of Mt Etna showing the location of the nine FLAME UV -Scanner station for near real-time automatic SO_2 flux measurements.
Figura 37 Mappa del Monte Etna che mostra l'ubicazione del 9 FLAME UV stazioni scanner per le misurazioni near real time automatiche del flusso di SO_2.

umn amounts are retrieved in real-time on site from the recorded UV open-path spectra applying the Differential Optical Absorption Spectroscopy (DOAS) technique but using a modeled clear-sky spectrum rather than a measured one as in the classic DOAS technique [Perner, 1983, Platt and Stutz, 2008; Salerno et al., 2009a].

Processed data is then transmitted via GSM telephonic modem links or WiFi to a Master Control Station located in the INGV Observatory in Catania, where the SO_2 flux is automatically computed and available for monitoring purposes [Salerno et al., 2009b; Bonaccorso et al., 2011; Calvari et al., 2011]. Uncertainty in computed flux ranges between -22 and +36% [Salerno et al., 2009b].

During ASI Prisma Campaign, the FLAME network has provided daylight SO_2 flux measurements from ~7:30 to ~16:00 (all times are in GMT) allowing a direct overlap with other data collected during the campaign, especially during the passage of the satellites TERRA and EO-1 over Mt Etna on 25 June 2012. On 25 June 2012, SO_2 flux and showed an average of ~ 1800 t d^{-1} with a standard deviation of 620 t d^{-1} (1 σ) enveloped between a minimum and maximum flux of 700 t d^{-1} (10:30) and 3000 t d^{-1} (13:35) respectively (Figure 38).

Figure 39 shows a SO_2 cross-section profile measured in the vertical plane above the ENIC station in Nicolosi at 10:00.

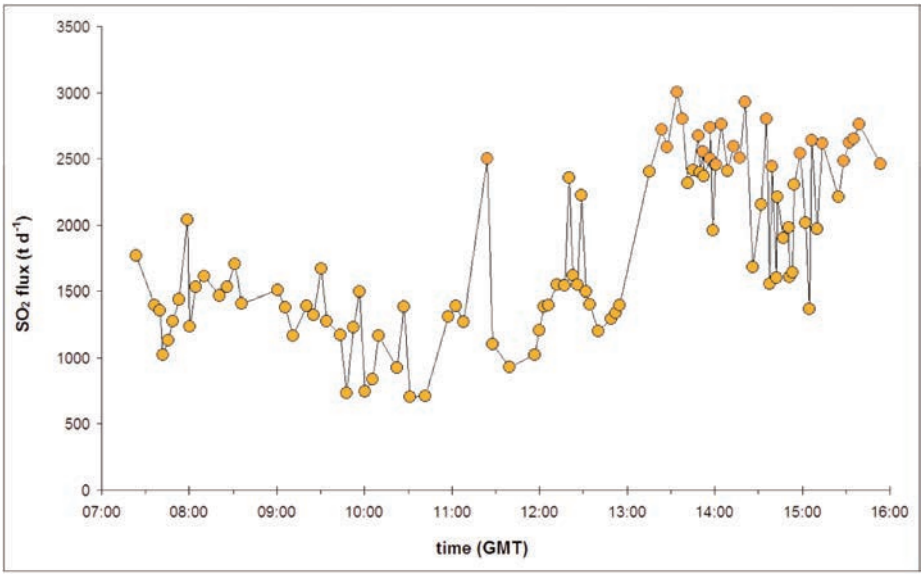

Figure 38 SO_2 Flux measured by FLAME network on 25 June 2012. During the day the flux showed a significant increasing trend starting at 13:00.
Figura 38 Flusso di SO_2 misurato dalla rete FLAME il 25 giugno 2012. Durante il giorno il flusso ha mostrato un andamento crescente significativo alle 13:00.

Table 15 reports the SO_2 flux data recorded by the FLAME network in overlap with the passage of ASTER and Hyperion satellites on 25 June 2012.

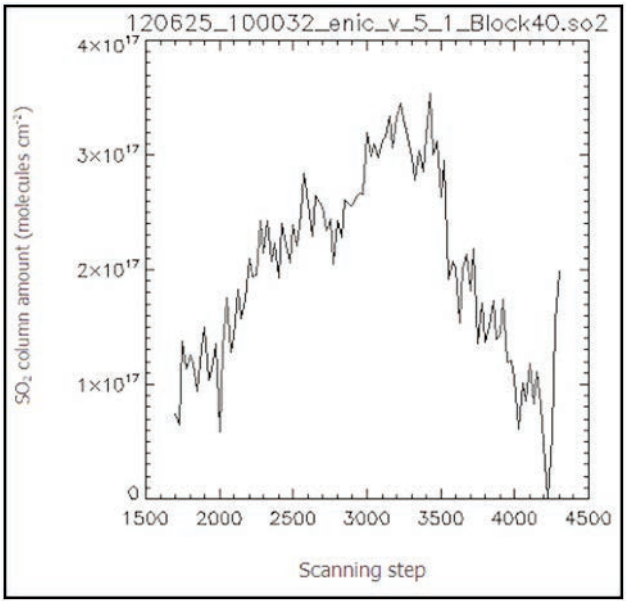

Figure 39 SO_2 column amount vs scanning step of a complete cross section profile measured by the ENIC station.
Figura 39 Colonna di SO_2 vs scanning step di un completo profilo di cross section misurato dalla stazione ENIC.

5.6 Atmospheric characteristics measurements

5.6.1 Multi-parametric meteo ground station

Since 2003, the remote sensing group has developed an integrated system to measure at ground many meteorological parameters in order to characterize the selected site. The fieldworks are always planned synchronously with a known satellite pass and a scheduled airborne flight. When this is established a ground based multi-parametric station is deployed to register many parameter within a temporal windows covering the satellite and airborne pass.
The home made portable ground station (Figure 41) is divided in 3 conceptual blocks represented in Figure 40.

- **Power supply** (**Green**): Essentially composed of 2 12 Volts/ 20 Watts (x2) solar panels which power is regulated by a homemade multi-plug-voltage power dispatcher, which acts as regulator and power distributor for all the devices used by the ground station. The power is backed up using a 12 Volts Battery. The solar panels disposed in parallel, can ensure battery charging during all the period of the survey
- **Sensors block** (**Blue**): This block takes in charge the acquisition of all the needed parameters to allow the following necessary atmospheric corrections on the remote sensed data from satellite and airborne. All the data are acquired thanks to a homemade PC Software "***Unilogger***" and all synchronized and geographically located thanks to a handheld GPS. The acquired parameters are the following:

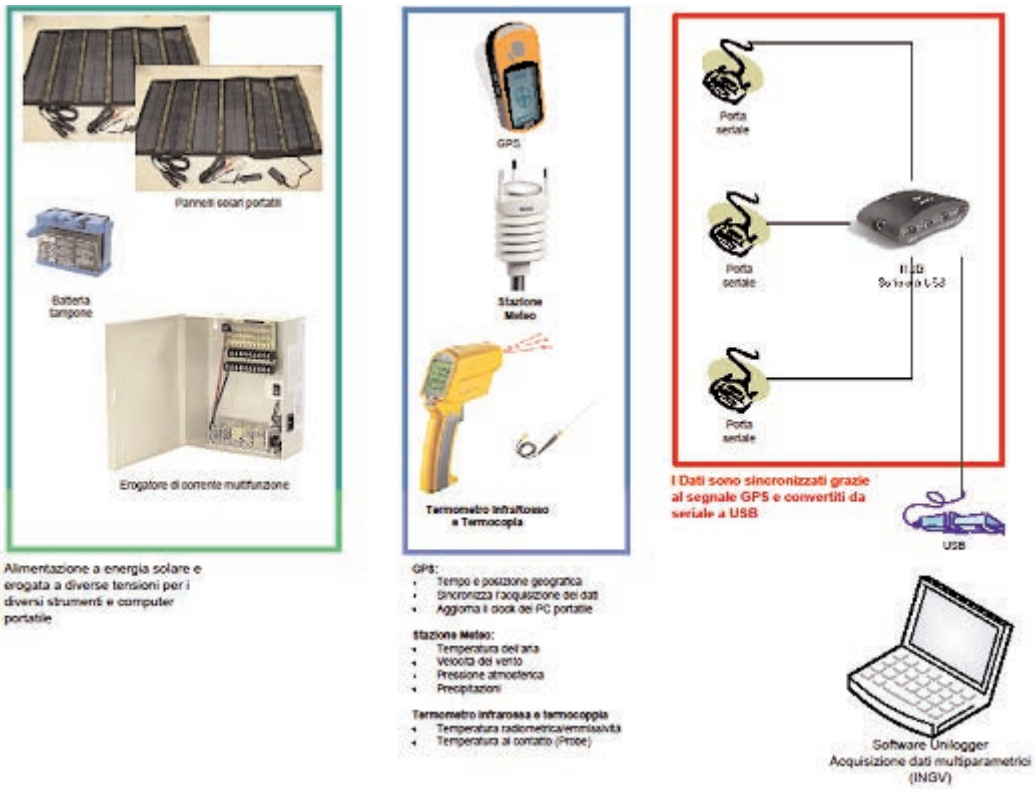

Figure 40 The three blocks (green, blu and red) composing the home made portable ground station.
Figura 40 I 3 blocchi (verde, blu e rosso) che compongono la stazione di terra portatile.

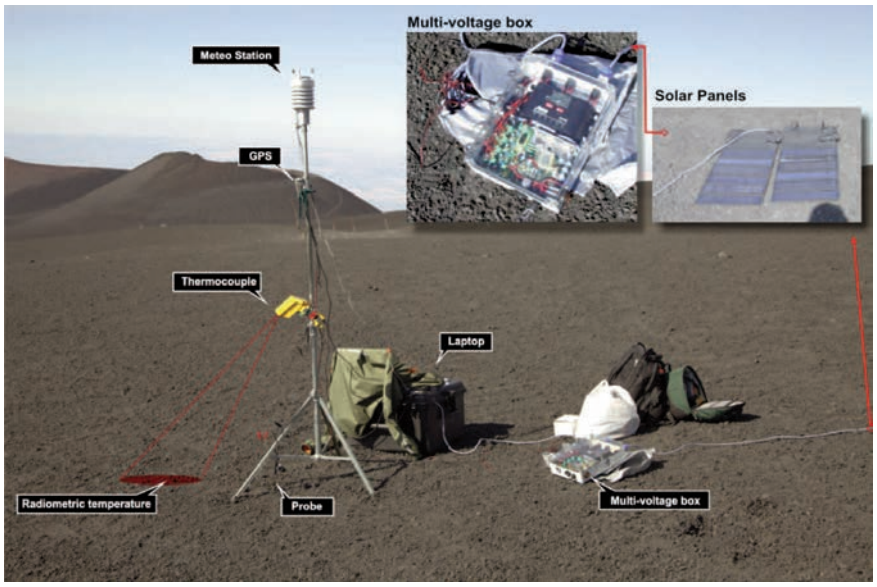

Figure 41 Home made portable ground station.
Figura 41 Stazione di terra portatile.

- **GPS**: UTC Time and Geographic position (Lat., Lon, Altitude). The GPS Time stamp is used for tagging the measures and synchronizing the PC clock.
- **Meteo**: Surrounding air temperature, Wind velocity, Atmospheric pressure, Precipitation.
- **Infrared Thermometer and Thermocouple Temperature**: Radiometric temperature / emissivity and soil contact thermocouple Temperature using a supplied probe.

- **Connectivity and computing Block** (**Red**): All the instruments are connected to a laptop through a Serial/USB hub converter and managed by our ***Unilogger*** software. It is a Visual Basic (VB.Net) software with a user friendly interface that takes care of handling the data input through the serial ports and synchronizing them in order to save them in ASCII files to be easily read or imported by several software.

The measurements were executed during the airborne and satellite acquisitions.

The temperature measured by the Fluke IR thermometer and by the probe shows the trend represented in Figure 42.

5.6.2 Sunphotometer observations

During the campaign sun-photometric measurements were performed in different places in order to characterize the atmospheric particulate. Sun-photometry permits to determine the total atmospheric optical thickness. Total optical thickness is the sum of the air molecules scattering (Rayleigh), of the aerosols scattering and of the ozone absorption in the wide Chappuis band. Water vapor and other gases may be neglected in the aerosols sun-photometer channels., while a dedicated channel of the photometer is generally used to determine the water vapor content.

The sun-photometers used is the portable MICRTOPS II model Solar Light. The instrument is a Volztype photometer with a 2.5° filed of view. Thanks to its reduced dimension and weight it is largely used in field campaigns also in volcanic areas (Figure 43). The instrument measure the sun radiance in a reduced field of view in the following wavelength channels: 440nm, 675nm, 870nm, 936nm and 1020nm.

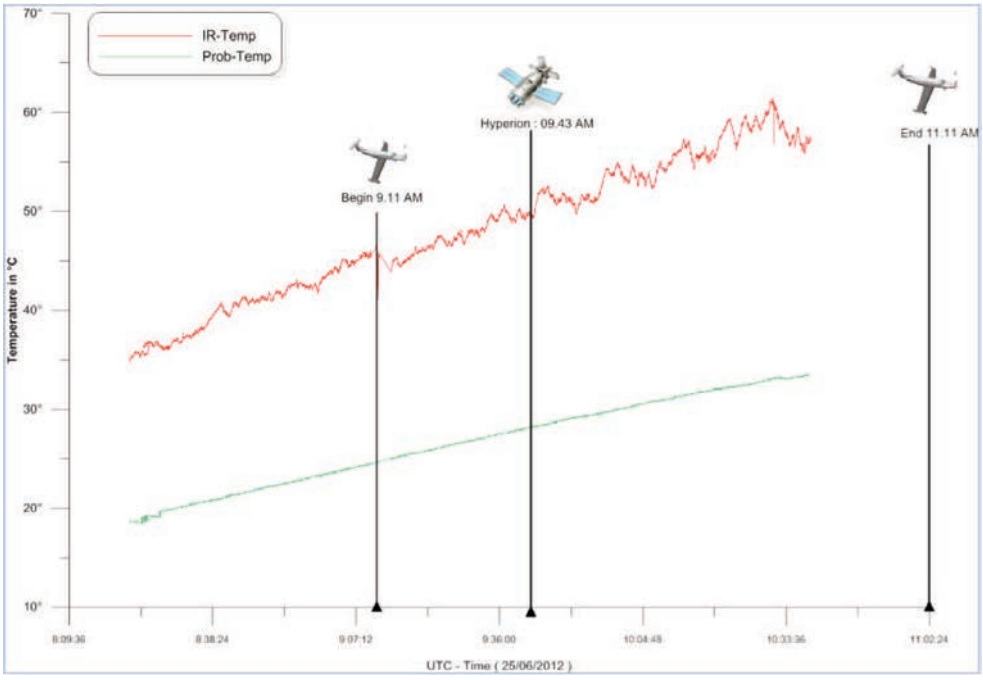

Figure 42 Temperature trend during the 25/06/2012 measurements.
Figura 42 Andamento della temperatura durante le misurazione del 25 giugno 2012.

MICROTOPS II provides the measurements of the Total optical thickness as a function of the wavelength and the water vapor columnar content.
In Table 16 the measurements executed are reported. In Figure 44 a sample of AOT measurements in 5 wavelength channel sampling the volcanic plume area and the atmospheric background are shown.

5.6.3 High resolution "Chemical Weather" forecast

The "chemical weather" is defined as the state of the atmospheric composition at given time. The term is borrowed from the definition of "weather", that defines the physical state of the atmosphere at a given time. CETEMPS in recent years implemented one operational system for chemical weather forecast over Europe and Italy [Menut and Bessagnet, 2010; Curci e Visconti, 2011; Curci, 2012; Zhang et al., 2012]. An experimental service, called ForeChem, automatically provides daily prediction of the concentration of pollutants (such as particulate matter, ozone and nitrogen dioxide) for the same day and the two subsequent days mak-

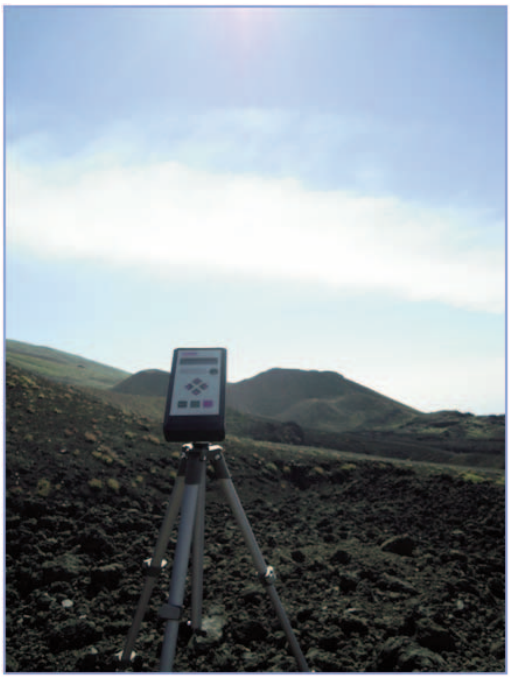

Figure 43 Sun-photemeter MICROTOPS II.
Figura 43 Fotometro solare MICROTOPS II.

DAY	START (UT)	STOP (UT)	MICRTOPS II Records	Altitude (m a.s.l.)	Coordinate	SITE
24-06-12	07.31	07.33	5	2023	37°42'17.2''N 15°00'07.9''E	Sapienza
24-06-12	08.29	08.36	8	2636	37°42'31.5''N 15°00'18.0''E	N Cone 2001
24-06-12	09.06	09.10	8	2743	37°44'01.6''N 15°00'28.9''E	W Cone 2002-2003
24-06-12	09.38	09.44	15	2839	37°44'18.9''N 15°00'27.8''E	SE ESNL
24-06-12	10.26	10.32	10	2939	37°44'18.9''N 15°00'27.8''E	Torre del Filosofo
25-06-12	08.04	08.11	10	1696	37°41'33.6''N 14°58'09.1''E	Forestal reserve
25-06-12	08.49	08.50	5	1765	37°42'21.1''N 14°57'45.5''E	2002 Lava flow
25-06-12	09.32	09.47	13	1859	37°43'20.9''N 14°57'21.3''E	1641 Lava field
26-06-12	07.35	07.50	15	210	37°34'23.7''N 14°53'24.5''E	Salinelle Paternò
26-06-12	08.20	08.26	9	207	37°34'23.1'N 14°53'24.6'E	Salinelle Paternò
26-06-12	13.44	13.58	25	928	37°44'04.5'N 15°06'10.5'E	Musco Street Milo
27-06-12	07.39	08.31	26	823	37°44'18.2'N 15°06'50.4'E	Milo

Table 16 Sun-photometer measurements sites.
Tabella 16 Siti di misura del fotometro solare.

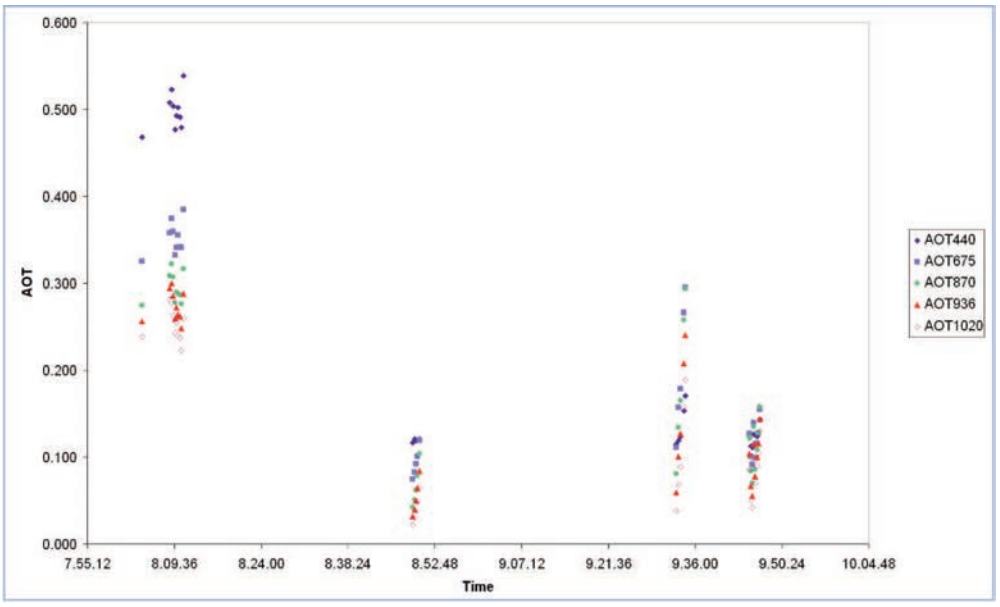

Figure 44 Total optical thickness trend obtained by sampling the volcanic plume and the atmosphere at three different sites along the Forest Reserve road. The optical thickness is represented as a function of the wavelength measurements acquired on 25th June 2012.
Figura 44 Andamento dello spessore ottico totale ottenuto campionando l'atmosfera ed il plume vulcanico in 3 siti ubicati lungo la strada della Riserva della Forestale. Lo spessore ottico è rappresentato come funzione delle misurazioni di lunghezza d'onda acquisite il 25 giugno 2012.

ing output available in graphical format on the web (http://pumpkin.aquila.infn.it/forechem/). Especially useful may be the forecast of the violations of thresholds for those pollutants regulated by the European Union as target to warrant a good quality of air [EC, 2008].

The concentration of chemical compounds in the atmosphere is regulated by four main categories of processes: emission, transport, chemical transformation, and deposition. Three-dimensional numerical models of the atmosphere contain a mathematical representation of our current knowledge on those processes and predicts the evolution in time and space of chemical species in the atmosphere. The models we will be talking about are called Chemistry-Transport Models (CTM). The data flow in a generic CTM at the regional scale (simulating a limited area, not the entire globe) is sketched in Figure 45. Given a set of meteorological fields, natural and anthropogenic gridded emission fluxes, land use map, and lateral boundary conditions the core of the model solves the set of differential equations that governs the concentration of chemical species. With a simplified mathematical notation, the CTM solves the set of coupled continuity equations for the considered chemical species:

$$\frac{\partial C_i}{\partial t} = -\mathbf{U}\cdot\nabla C_i + P_i - D_i \qquad \{i = 1,\ldots,n\}$$

where C_i is the molar fraction of the i-th species, t is time, $\mathbf{U}$ is the wind vector, P_i and D_i the production and destruction terms of C_i, n is the number of chemical species. The first term on the right hand side denotes the processes of transport (advection, turbulent diffusion, etc.). P_i and D_i include emissions, chemical production/destruction and deposition.

The meteorological input to the ForeChem system is currently provided with the MM5 model [Dudhia, 1993]. Simulations domains are two, one covering Central-Western Europe at an horizontal resolution of 36 km and another nested into the first that covers Italy at a resolution of 12 km. In the vertical, the model has 29 sigma levels (i.e. pressure levels that smoothly follow the topography) from ground to about 18 km with a resolution that degrades from bottom to top. In the first 200 m there are 4 levels, in the first 1 km there are 10 levels.

The chemistry-transport model used in ForeChem is CHIMERE [Bessagnet et al., 2008]. It is also setup on two nested domains, the first over Europe with a resolution of 0.5° (about 45 km) and the other nested over Italy at 0.15° resolution (about 12 km). In the vertical the model goes from ground to 500 hPa (5.5 km) with 8 sigma levels. The anthropogenic emissions of the species of interest (carbon monoxide, oxides of nitrogen, sulphur dioxide, non-methane hydrocarbons, ammonia and particulate matter) is derived from the inventory provided by the Environmental and Monitoring Evaluation Program (EMEP http://www.ceip.at/emission-data-webdab/emissions-used-in-emep-models/) for the European scale and from the inventory of Centro Tematico Nazionale su Ambiente Clima ed Emissioni (CTN-ACE) for the Italian scale. Biogenic emissions of hydrocarbons are calculated with the MEGAN model [Guenther et al., 2006]. The model simulated the main tropospheric chemical reaction in the gas and heterogeneous phase (about 80 species and 200 reactions) at the base of the ozone-oxide of nitrogen-hydrocarbons chemistry [Jenkin and Clemitshaw, 2000]. Aerosol [Poschl, 2005] are

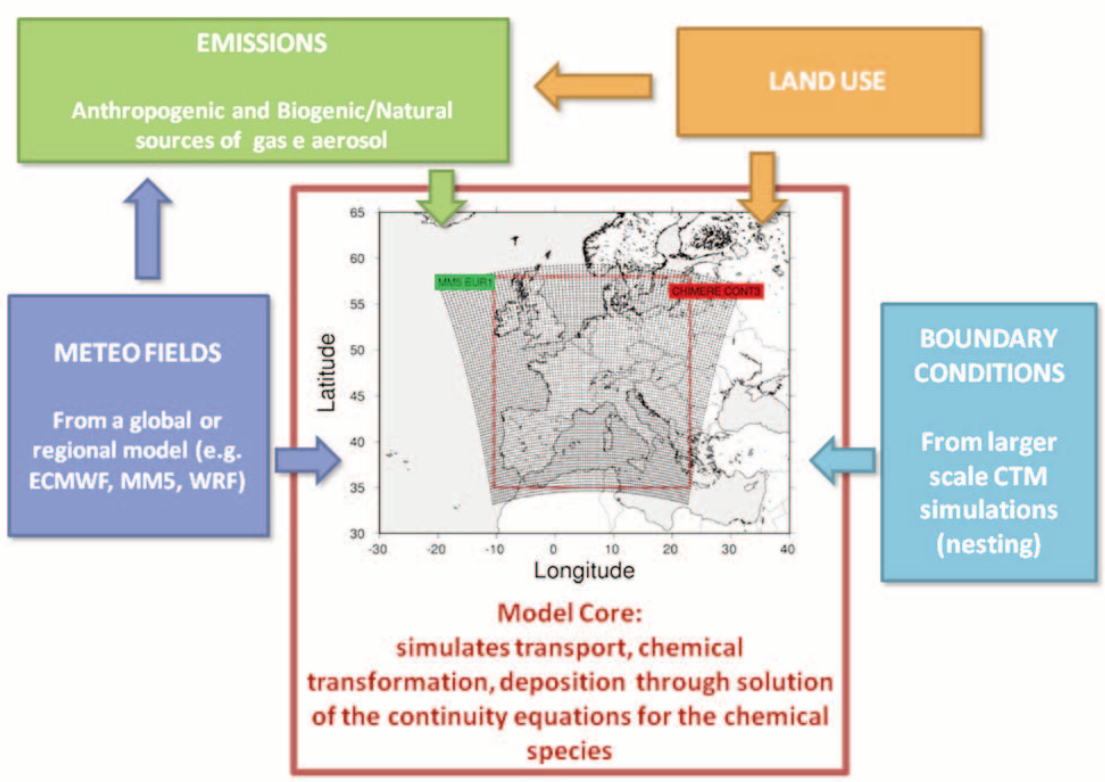

Figure 45 Data flow in a Chemistry-Transport Model (CTM). In a CTM the processes governing the evolution of atmospheric chemical composition are solved over a three-dimensional discrete grid. Meteorological fields are produced offline with a meteorological model and passed as input to the CTM. Other main inputs are the emissions fluxes from natural and anthropogenic source, the land use map, and the lateral boundary conditions for chemical species.
Figura 45 Flusso di dati in un modello di chimica e trasporto (CTM). In un modello CTM si risolvono su una griglia discreta tri-dimensionale i processi che determinano l'evoluzione della composizione chimica atmosferica. I campi meteorologici non vengono calcolati direttamente nel CTM, ma sono forniti in ingresso dalla simulazione di un modello di circolazione generale o a scala regionale (GCM o RCM). Altri dati in ingresso sono i flussi di emissioni da sorgenti naturali o legati all'attività antropica e dati sull'utilizzo del suolo. Per i CTM ad area limitata (non globale, come in figura) sono necessarie in ingresso alle le concentrazioni chimiche al contorno del dominio simulato.

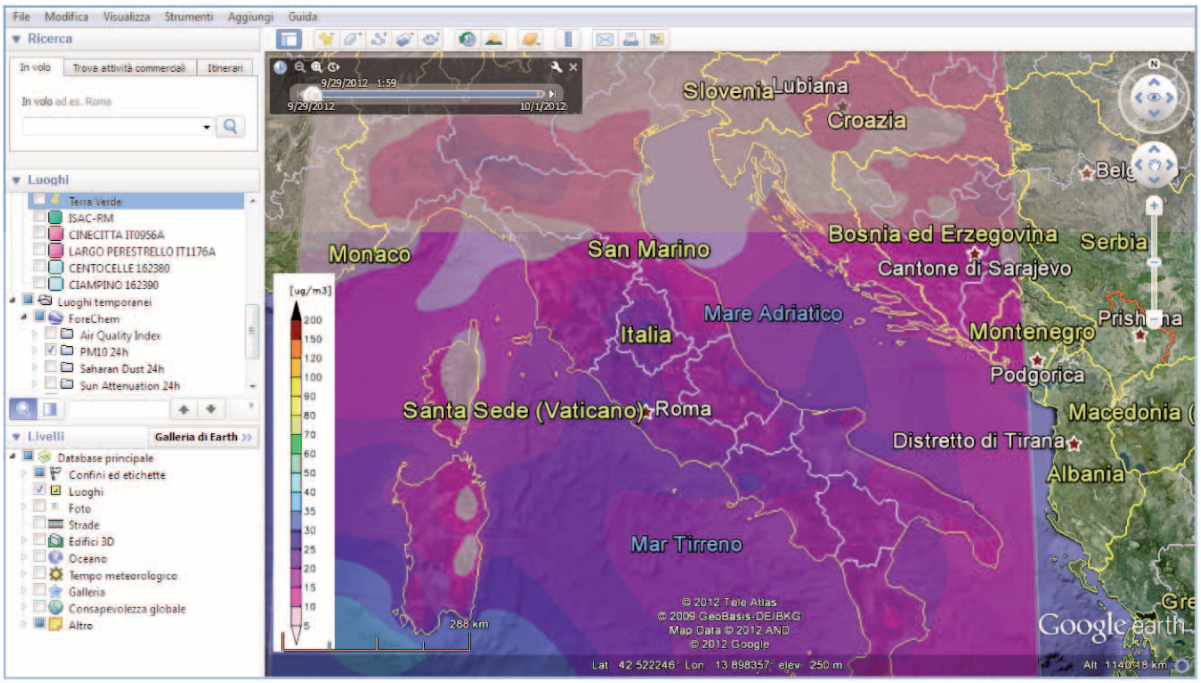

Figure 46 Screenshot of ForeChem forecast on Google Earth.
Figura 46 Esempio di visualizzazione delle previsioni ForeChem su Google Earth.

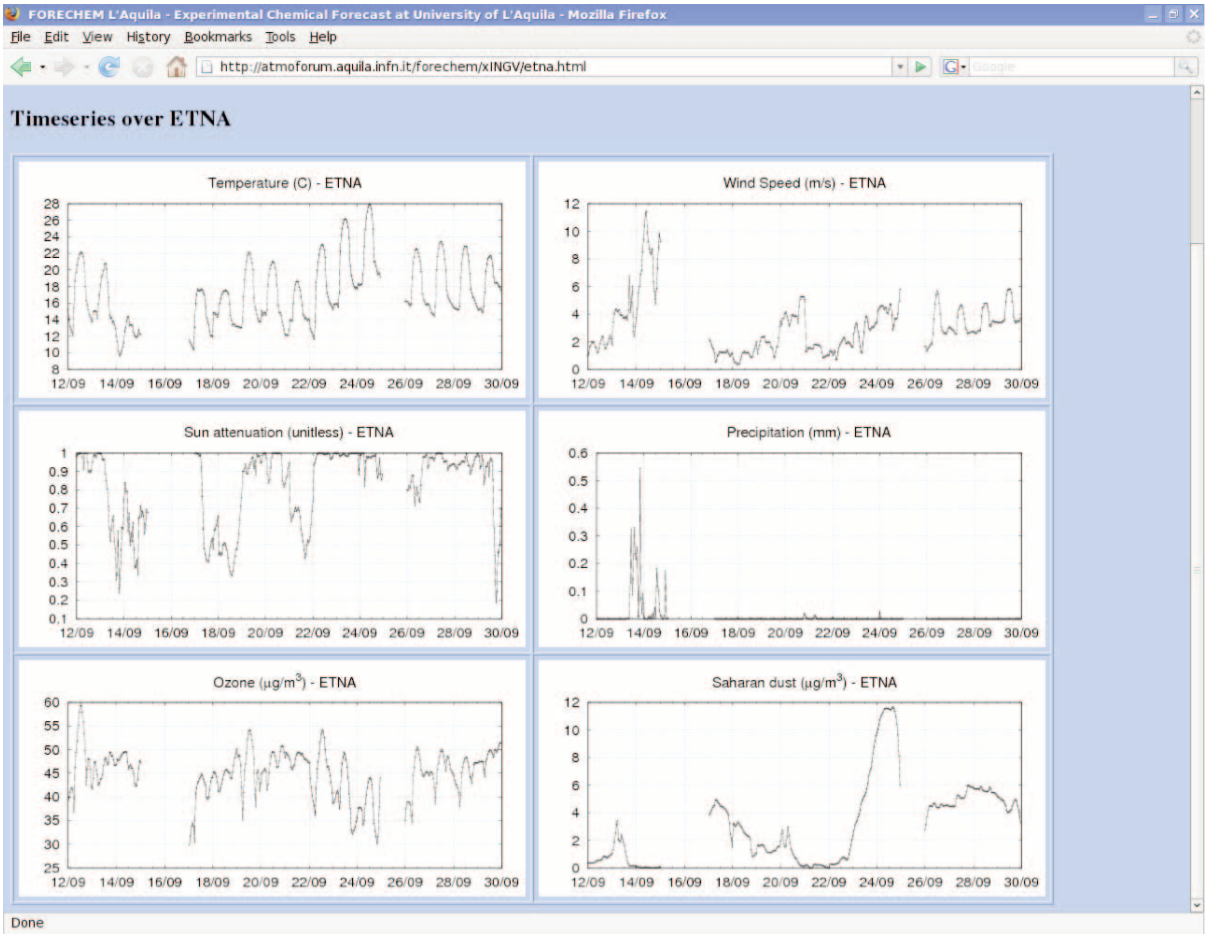

Figure 47 Screenshot of point output of ForeChem forecast over Mount Etna. From top to bottom the time series of selected variables for 14 days before and 2days ahead of: temperature, wind speed, sun attenuation, precipitation, ozone concentration, Saharian dust concentration.
Figura 47 Esempio di visualizzazione puntuale delle previsioni ForeChem sul monte Etna. Dall'alto verso il basso: temperatura, velocità del vento, attenuazione della radiazione solare, pioggia, concentrazione di ozono e concentrazione di polvere Saharian.

simulated with a section al model with 8 bins from 40 nm to 10 µm. For further details on the system and a synthesis of validation results the reader may refer to Curci [2012] and to the User's Guide of CHIMERE (http://www.lmd.polytechnique.fr/chimere/). On the Italian domain, the model overestimates on average the maximum daily ozone levels by 10% (correlation of 0.76) and underestimates the daily values of particulates with a diameter less than 10 µm (PM10) by 30-40% (correlation 0.5), in line with the state-of-the-art.
During the measurement campaign over Mount Etna new features to the ForeChem system were implemented in order to have a more flexible visualization of the output. The two developments concern the visualization of the maps on Google Earth and the output of variable timeseries at selected locations of interest. In Figure 46 we show an example of the Google Earth maps that may be visualized using the KMZ file at this link: http://pumpkin.aquila.infn.it/forechem/ge/forechem_ITA.kmz
while in Figure 47 we show a screenshot of the time series of Mount Etna, updated every day at the link:
http://pumpkin.aquila.infn.it/forechem/xINGV/etna.html
A web interface with fully customizable graphical output of the ForeChem chemical weather forecasts is currently under development.

Conclusions

The field campaign over Mt. Etna area was successfully completed according to the original planning also thanks to excellent weather conditions. Ground data collected will be used to calibrate and validate the airborne images acquired over the test sites. The ground spectral data set collected will also be processed to create a spectral library of Mt. Etna surface materials. The whole data set acquired during this campaign will be used to extract a suitable data set to simulate PRISMA data and to develop and test the algorithms in the frame of ASI-AGI project.

Aknowledgements

Mt Etna and Paternò field campaign 2012 was funded by the Agenzia Spaziale Italiana (ASI) in the frame of the research project ASI-AGI n. I/016/11/0. We thank Dr. David Pieri (NASA-Jet Propulsion Laboratory, ASTER Science Team) for the successfully acquisition and process of ASTER imagery during the field campaign. We also thank Dr. Elizabeth Middleton, Dr Stuart Frye and Dr Petya Campbell, Goddard Space Flight Centre for providing Hyperion data. We wish to thank all the colleagues from the Catania section of INGV, especially Dr Giuseppe Puglisi who kindly provided GPS data for airborne data geometric correction; we also thank the National Coast Guard for the remarkable support to the ground and water measurements activities during the campaign. Finally we are grateful to the editorial board of Quaderni di Geofisica for the accurate and patient work done and to Dr Stefano Corradini for his revision activity and his precious suggestions.

References

Acharya P.K., Berk A., Bernstein L.S., Matthew M.W., Adler-Golden S.M., Robertson D.C., Anderson G.P., Chetwynd J.H., Kneizys F.X., Shettle E.P., Abreu L.W., Galery W.O., Selby J.E.A., Clough S.A., (1998). *Modtran User's Manual, Versions 3.7-4.0*. Air Force Research Laboratory, Space Vehicles Directorate, Air Force Materiel Command, Hanscom AFB, MA 01731-3010.

Acocella V., Behncke B., Neri M., D'Amico S., (2003). *Link between major flank slip and eruptions at Mt. Etna (Italy)*. Geophysical Research Letters, 30: DOI: 10.1029/2003-GLO 18642.

Acocella V., Neri M., (2003). *What makes flank eruptions? The 2001 Etna eruption and the possible triggering mechanisms*. Bulletin of Volcanology, 65: 517-529, DOI: 10.1007/s00445-003-0280-3.

Aikio M., (2001). Hyperspectral *prism-grating-prism imaging spectrograph*. Espoo 2001, Technical Research Centre of Finland, VTT Publications 435.

Allard P.J., Carbonelle N., Mètrich H., Loyer P. & Zettwoog P., (1994). *Sulphur output and magma degassing budget of Stromboli volcano,* Nature, 368:326-330.

Allard P.J., Jean-Baptiste P., D'Alessandro W., Parello F., Parisi B. & Flehoc C., (1997). *Mantle-derived helium and carbon in groundwaters and gases of Mount Etna, Italy*. Earth and Planetary Science Letters, 148 : 501-516.

Andres R.J., Kyle P.R., Rose W.I., Stokes J.B., (1987). *SO_2 emissions during eruptive episode 48A, Kilauea Volcano, Hawaii*. IUGG XIX General Assembly: 407.

Andres R.J., Kyle P.R., Stokes J.B., Rose W.I., (1989). *SO_2 from episode 48A eruption, Hawaii : Sulfur dioxide emission from the episode 48A east rift zone eruption of Kilauea volcano, Hawaii*. Bull. Volcanol., 52 : 113-117.

Andronico D. et al., (2004). *A multi-disciplinary study of the 2002-03 Etna eruption: insights for into a complex plumbing system.* Bulletin of Volcanology.

Armienti P., Clocchiatti R., D'Orazio M., Innocenti F., Petrini R., Pompilio M., Tonarini S., (1994). *Etna petrography and chemical composition*. Acta Vulcanol., 6: 3-5.

Badalamenti B., Calderone L., Liotta M., Sansone G., (1999). *Continuous monitoring.* Volcanology and Chemistry of the Earth's interior – Italian Research Activity (1995-1998) report to IAVCEI, Boll. Geol. Teor. Appl., 40-2 supplement: pp.214-216.

Barberi F., Innocenti F., Ferrara G., Keller J., Villari L., (1974). *Evolution of Aeolian Arc Volcanism (Southern Tyrrhenian Sea)*. Earth Planet. Sc. Lett., 21: 269-276.

Barberi F., Neri G., Valenza M., Villari L.,(1990). *Italian volcanic activity during 1987-1990. Volcanological research in Italy (1987-1990)*. F. Barberi ed., Boll. Geof. Teor. Appl., Supplement vol. 32: 127-128, 427-445.

Barnaba F., Gobbi G.P., (2001). *Lidar estimation of tropospheric aerosol extinction, surface area and volume: Maritime and desert-dust cases*. J. Geophys. Res., 106 (D3), 3005-3018.

Behncke B., Neri M., (2003a). *The July-August 2001 eruption of Mt. Etna (Sicily)*. Bulletin of Volcanology 65: 461-476, DOI: 10.1007/s00445-003-0274-1.

Behncke B., Neri M., (2003b). *Cycles and trends in the recent eruptive behaviour of Mount Etna (Italy)*. Canadian Journal of Earth Sciences 40: 1405-1411, DOI: 10.1139/E03-052.

Behncke B., Neri M., Carniel R., (2003). *An exceptional case of lava dome growth spawning pyroclastic avalanches at Mt. Etna (Italy): the 1999 Bocca Nuova eruption*. Journal of Volcanology and Geothermal Research 124: 115 - 128.

Behncke B., Berrino G., Velardita R., (2003). *Ground deformation and gravity changes on the island of Pantelleria in the geodynamic framework of the Sicily channel* (invited press). Abstract presented at the Annal Workshop 2003, Pantelleria, Italy (23-28 September 2003). on : Seismic Phenomena Associated with Volcanic Activity (view abstract).

Bessagnet B., Menut L., Curci G., Hodzic A., Guillaume B., Liousse C., Moukhtar S., Pun B., Seigneur C.and Schulz M., (2008). *Regional modeling of carbonaceous aerosols over Europe - Focus on Secondary Organic Aerosols.*Journal of Atmospheric Chemistry, 61, 175-202.

Billi A., Acocella V., Funiciello R., Giordano G., Lanzafame G., Neri M., (2003). *Mechanisms for ground-surface fracturing and incipient slope failure associated to the July-*

August 2001 eruption of Mt. Etna, Italy: analysis of ephemeral field data. Journal of Volcanology and Geothermal Research 122: 281-294.

Bluth G.J.S., Shnetzel C.C., Kreuger A.J., Walter L.S., (1993). *Annual volcanic emission of sulfur dioxide to the atmosphere.* Eos Transaction AGV, 74 : 688.

Bonaccorso A., Caltabiano T., Currenti G., Del Negro C., Gambino S., Ganci T., Giammanco S., Greco F., Pistorio A., Salerno G., Spampinato S. and Boschi E., (2011). *Dynamics of a lava fountain revealed by geophysical, geochemical and thermal satellite measurements: the case of 10 April 2011 Mt. Etna eruption*. Geophys. Res. Lett., 38, L24307, doi:10.1029/2011GL049637.

Briess K., Jahn H., Lorenz E., Oertel D., Skrbek W., Zuhkov B., (2003). *Fire recognition potential of the Bi-spectral InfraRed Detection (BIRD)satellite.* Intern. Journ. Remote Sensing.

Bruno N., Caltabiano T., Romano T., (1999). *SO(sub2) emissions at Mount Etna with particular reference to the period 1993-1995*. Bulletin of Volcanology. 7 (1): 27-34.

Burton M.R., Oppenheimer C., Horrocks L.A., Francis P.W., (2000). *Remote sensing of CO_2 and H_2O emission rates from Masaya volcano, Nicaragua*. Geology, 28: 915-918.

Burton M.R., Murè F., Sawyer G., Allard P., (2003). *FTIR measurements of 2002/2003 flank eruption of Mt. Etna*. EGS-AGU-EUG joint Assembly, Nice.

Caltabiano T., Romano R., Buretta G., (1994). *SO_2 flux measurements at Mount Etna*. J. Geophys. Res. 99 (D6): 809-819.

Carbonnelle J., Dajlevic D., Zettwoog P., Sabroux J.C., (1982). *Gas output measurements from an active volcano.* Bull. Volcanol., 45 : 267-268.

Casadevall T.J., Stokes J.B., Greenland L.P., Malinconico L.L., Casadevall J.R., Furukawa B.T., (1987). *SO_2 and CO_2 emission rates in Kilauea volcano,* 1979-1984, chap. 29 in: Decker, R. W., Wright, T.L. and Stauffer, P. H. eds., Volcanism in Hawaii : U.S. Geological Survey Professional Paper 1350: vol. 1, pp. 771-780.

Chartier T.A., Rose W.I., Stokes J.B., (1998). *Detailed record of SO_2 emissions from PUU Oo between episodes 33 and 34 of the 1983-1986 ERZ eruption, Kilauea, Hawaii*. Bull. Volcanol., 50 : 215-228.

Chiodini G., Cioni R., Guidi M., Raco B. and Marini L., (1998). *Soil CO_2 measurements in volcanic and geothermal areas*. Appl. Geochem. 13-5: 543-552.

Cristofolini R., Lentini F., Patanè G., Rasà R., (1979). *Integrazione di dati geologici, geofisici e petroglifici per la stesura di un petroglifo crostale in corrispondenza dell'Etna*. Boll. Soc. Geol. It., 98: 239-247.

Curci G., (2012). *An Air Quality Forecasting tool over Italy (ForeChem), in Air Pollution Modelling and its Application*. XXI, Edited by Douw G. Steyn and Silvia Trini Castelli, ISBN 978-94-007-1358-1.

Curci G., and Visconti G., (2011). *Modelli e dati per lo studio dei cambiamenti climatici e la qualità dell'aria*. Rivista Abruzzese, Rassegna Trimestrale di Cultura, Jun 2011, ISBN 978-88-96804-15-5.

Diliberto I.S., Gurrieri S., Valenza M., (2002). *Relationships between diffuse CO_2 emissions and volcanic activity on the island of Vulcano (Aeolian Islands, Italy) during the period 1984-1994*. Bulletin of Volcanology, 64: 219-228.

Dudhia J., (1993). *A nonhydrostatic version of the Penn State/NCAR mesoscale model: Validation tests and simulation of an Atlantic cyclone and cold front*. Mon. Wea. Rev., 121, 1493–1513.

EC (2008). *Directive 2008/50/EC of the European Parliament and of the Council of 21 May 2008 on ambient air quality and cleaner air for Europe.*

Elias T., Sutton A.J., Tokes J.B., Casadevall T.J., (1998). *Sulfur dioxide emission rates of Kilauea Volcano, Hawaii*. 1979-1997. U.S. Geological Survey Open-File Report 98-462.

Favalli M., Fornaciai A., Isola I., Tarquini S., Nannipieri L., (2012). *Multi-View 3D reconstruction in geosciences*. Computer & Geosciences, 44, 168-176, doi:10.1016/j.cageo.2011.09.012.

Favara R., Francofonte S., Madonia P. and Valenza M., (1997). *Modello idrogeologico dell'Isola di Vulcano e suo significato per la sorveglianza geochimica*. In: C.N.R./G.N.V., Convegno Annuale 1996, 3-5 Marzo 1997, Programma e Riassunti, pp. 162-163, Roma.

Francis P., Maciejewski A., Oppenheimer C., Caltabiano T. (1995). *SO_2: HCL ratios in the plumes from Mt. Etna and Vulcano determined by Fourier Transform Spectroscopy.* Geophysical Research Letters 22: 1717-1720.

Francis P., Burton M. & Oppenheimer C., (1998). *Remote measurements of volcanic gas compositions by solar FTIR spectroscopy.* Nature, 396 : 567-570.

Furukawa Y., Ponce J., (2009). *Accurate camera calibration from multi-view stereo and bundle adjustment*. International Journal of Computer Vision 84, 257–268.

Gobbi G.P., (1998). *Polarization lidar returns from aerosols and thin clouds: a framework for the analysis*. Appl. Opt., 37, 5505–5508.

Gobbi G.P., Barnaba F., Giorgi R., Santacasa A., (2000). *Altitude-resolved properties of a Saharian-Dust event over the Mediterranean.* Atmospheric Environment, 32 : 5119-5127.

Guenther A., Karl T., Harley P., Wiedinmyer C., Palmer P. I., and Geron C., (2006). *Estimates of global terrestrial isoprene emissions using MEGAN (Model of Emissions of Gases and Aerosols from Nature)*. Atmos. Chem. Phys., 6, 3181-3210

Gurrieri S. and Valenza M., (1988). *Gas transport in natural porous medium: a method for measuring CO_2 flows from the ground in volcanic and geothermal areas.* Rendiconti

della Società Italiana di Mineralogia e Petrologia, 43: 1151-1158.

Haulet R., Zettwoog P., Sabroux J.C., (1977). *Sulfur dioxide discharge from Mount Etna*. Nature, 268: 715-717.

Hoff R.M., Millan M.M., (1981). *Remote SO_2 mass flux measurements using COSPEC*. Air Pollut. Control Assoc., 31: 381-384.

Jaeschke W., Berresheim H., and Georgii H.W., (1982). *Sulfur emission from Mount Etna*. J.Geophys. Res., 87 (C9):7253-7261.

Jenkin M.E., and. Clemitshaw K.C., (2000). *Ozone and other secondary photochemical pollutants: chemical processes governing their formation in the planetary boundary layer*. Atmospheric Environment, 34, 2499-2527.

Keller J., (1980). *The island of Vulcano*. Soc. Italiana Min. Petr.; 36: 368-413.

Krueger A.J., Schaefer S.J., Krotkov N., Bluth G., and Barker S., (2000). *Ultraviolet remote sensing of volcanic emissions*. in Remote Sensing of Active Volcanism, edited by P.J. Mouginis-Mark, J.A. Crisp, and J.H. Fink, pp. 25-43, Geophysical Monograph 116, AGU, Washington,D.C.

Lanzafame G., Neri M., Acocella V., Billi A., Funiciello R., Giordano G., (2003). *Structural features of the July-August 2001 Mount Etna eruption: evidence for a complex magma supply system*. Journal of the Geological Society London 160: 531-544.

Lenoble J., (1993). *Atmospheric Radiative Transfer. (*studies in Geophysical Optics and Remote Sensing). A. Deepak Pub., May 1.

Lorenz E., Skrbek, W., (2001). *Calibration of a bi-spectral infrared push-broom imager*. Proc. SPIE: 4486: 90-103.

Lundgren P., Berardino M., Coltelli M., Fornaro G., Lanari R., Puglisi G., Sansosti E., Tesauro M., (2003). *Volcanic sulphur dioxide fluxes from Etna, Vulcano and Stromboli measured with an automated scanning ultraviolet spectrometer*. J. Geoph. Res.:108, B9, 2455.

Malinconico L.L., (1979). *Fluctuations in SO_2 emission during recent eruptions of Etna*. Nature, 278: 43-45.

Malinconico L.L., (1987). *On the variation of SO_2 emissions from volcanoes*. J. Volcanol. Geotherm. Res., 33: 231-237.

Mazzarini F., Favalli M., Isola I., Neri M., Pareschi M.T., (2008). *Surface roughness of pyroclastic deposits at Mt. Etna by 3D laser scanning*. Annals of Geophysics, 51, 5/6, 813-822.

Menut L., Bessagnet B., (2010). *Atmospheric composition forecasting in Europe*. Ann. Geophys., 28, 61-74.

Mercalli G., Silvestri O., Gblovitz G., Clerici V., (1891). *L' eruzione dell'Isola di Vulcano*. Annali dell'Ufficio centrale di metereol., 10: pt. 4.

Millan M.M., (1984). The *applications of Optical Correlation Techniques to the Remote Sensing of Air Pollution*. P. Camagni, S. Sandroni (eds.), Elsevier Pub. Co., New York: 45-67.

Millan M.M., (1978). *Remote sensing of SO_2, a data processing methodology*. Joint Conference on Sensing of Environmental Pollutants. 4th New Orelans, La. Nov. 6-11, 1977, Proceedings. (A79-15023 04-45) Washington, D.C., American Chemical Society, pp. 30-33.

Millan M.M., Hoff R.M., (1977). *How to minimize the baseline drift in a COSPEC remote sensing*. Journal of Atmoshperic Environment vol. 11: n°9, pp. 857-860.

Moffat A.J., Millan M.M., (1971). *The applications of optical correlation techniques to the remote sensing of SO_2 plume using sky light*. Atmos. Environn., 5:677-690.

Neri M., Acocella V., Behncke B., (2003). *The role of the Pernicana Fault System in the spreading of Mount Etna (Italy) during the 2002-2003 eruption*. Bulletin of Volcanology, DOI: 10. 1007/s00445-003-0322-x.

Newcomb G.S., Millan M.M., (1970). *Theory, applications, and results of long-line correlation spectrometer*. IEEE Trans. Geosci. Electron., GE 8: 149-157.

Parkinson K.J., (1981). *An improved method for measuring soil respiration on the field*. J. Appl. Ecol. 18: 221-228.

Poschl U., (2005). *Atmospheric Aerosols: Composition, Transformation, Climate and Health Effects*. Angewandte Chemie Int. Ed., 44, 7520-7540.

Rittmann A., (1958). *Sul meccanismo dell'attività vulcanica persistente*. Bollettino dell'Accademia Gioenia di Scienze Naturali di Catania, ser. IV, 4: 352-360.

Rittmann A., (1962). *On the mechanism of persistent volcanic activity*. Bulletin Volcanologique 24 : 301-313.

Romano R., Vaccaro C. (1986). *The recent eruptive activty on Mt. Etna, Sicily: 1981-1985*. Per. Mineral. 55 : 91-111.

Romano R. (1982). *Succession of the volcanic activity in the Etnean area*. Mem. Soc. Geol. It., 23: 27-48.

Rothman L.S., Rinsland C.P. et al. (1998). *The HITRAN Molecolar Spectroscopic Database and HAWKS (HITRAN Atmospheric Workstation)*. 1996 Edition, Journal of Quantitative Spectroscopy and Radiative Transfer, 60: 665-710.

Salerno G.G., Burton M.R., Oppenheimer C., Caltabiano T., Tsanev V. and Bruno N. (2009a). *Novel retrieval of volcanic* SO_2 abundance from ultraviolet spectra. J. Volcanol. Geot Res. 181,141-153. doi:10.1016/j.jvolgeores.2009.01.009.

Salerno G. G., Burton M.R., Oppenheimer C., Caltabiano T., Randazzo D., Bruno N., Longo V. (2009b). *Three-years of SO_2 flux measurements of Mt. Etna using an automated UV scanner array: Comparison with conventional traverses and uncertainties in flux retrieval*. J. Volcanol. Geotherm. Res., 183, 76-83, doi 10.1016/j.jvolgeores.2009.02.013.

Shepard M.K., Campbell B.A, Bulmer M.H., Farr T.G.,

Gaddis L.R. and Plaut J.J. (2001). *The roughness of natural terrain: A planetary and remote sensing perspective*. J. Geophys. Res., 106, 32777-32795.

Skrbek W., Lorenz E. (1998). *HSRS – An infrared sensor for hot spot detection*. Proc. SPIE: 3437: 167-176.

Snavely, N., Seitz, D., Szeliski, R., (2007). *Modeling the world from internet photo collections.* International Journal of Computer Vision 80, 189–210.

Snavely, N., Seitz, S.M., Zeliski, R.S., (2006). *Photo tourism: Exploring image collections in 3D*. In: SIGGRAPH Conference Proceedings, New York, NY, USA, ACM Press, pp. 835–846.

Stoiber R.E., Malinconico L.L, Williams, Jr S.N., (1983). *Use of correlation spectrometer at volcanoes.* In Forecasting Volcanic events, H. Tazieff & J-C Sabroux (eds) 425-44. Amsterdam Elsevier.

Sutton A., Elias T., Gerlach T., and Stokes J., (2001). *Implications for eruptive processes as indicated by sulfur dioxide emissions from Kilauea Volcano, Hawaii, 1979 – 1997*. Journal of Volcanology and Geothermal Research, no. 108: pp. 283-302.

Sutton J., Elias T., Hendley J.W.I., Stauffer P.H., (1997). *Volcanic air pollution – a hazard in Hawaii*. U.S. Geological Survey fact Sheet: 169-97 (Reducing Rirsk from Volcano Hazards series), p. 2.

Tanguy J.C.,(1978). Tholeitic *basalt magmatism of Mount Etna and its relations with the alcaline series.* Contrib. Mineral. Petrol., 66: 51-67.

Tonani F. and Miele G., (1991). *Methods for measuring flow of carbon dioxide through soils in the volcanic setting.* Proc. Int. Conf. Active Volcanoes and Risk Mitigation, 27 August-1 September, Napoli.

W.M.O., (1984). *W.M.O. Manual on Codes W.M.O.* vols 1 & 2: n° 306

Wooster M., Zhukov B., and Oertell D., (2003). *Fire Radiative energy release for quantitative study of biomass burning: derivation from the BIRD experimental satellite and comparison to MODIS fire products.*Remote Sens. Environm.

Zhang Y., BocquetM., Mallet V., Seigneur C., Baklanov A., (2012). *Real-time air quality forecasting, part I: History, techniques, and current status*. Atmospheric Environment, 60, 632-655.

Zhukov B., Briess K., Eckehard L., Skrbek W.,Oertel D., (2003). *Detection and Analysis of High-Temperature Events in the BIRD Mission.* DLR, Berlin.

ISSN 1590-2595
Anno 2014_Numero 119

annex A

Description of Mt Etna test site

Mount Etna is the largest and most active of Europe's volcanoes, with a present summit elevation of 3315 m, and eruptive activity occurring nearly every year. Eruptions occur both at the summit, where there are four craters (Northeast Crater, Voragine, Bocca Nuova, Southeast Crater) and on the flanks, of which more than 300 individual craters bear testimony. Summit activity may be continuous over many years or even decades, while flank eruptions occur every few years, with a clear trend towards an increase in the frequency of flank eruptions and in the long-term output rate being observed in the past 50 years or so. Since the late 1970s, summit eruptions have shown a clear increase in their intensity, and one hallmark of this activity has been the extremely high rate of short-lived, extremely violent paroxysmal eruptive episodes, which culminated in more than 120 paroxysms during the 6 years between 1995 and 2001, most of which occurred at the youngest of the summit craters, the Southeast Crater. Such events commonly produce lava fountains that reach heights of many hundred meters, in some cases exceeding 1000 m. Etna can even boast having produced the tallest lava fountain ever measured on any volcano, >2000 m, on 4 September 1999. Most lava fountains are accompanied by the generation of abundant tephra that consists of highly inflated scoriae and can fall tens of kilometers away from the volcano on the downwind side.In contrast to these impressive but brief (rarely more than 30 minutes) episodes, summit eruptive activity at other times occurs in a continuous but notably milder manner, sometimes for years without interruption. This is what once was believed to be the most characteristic activity at

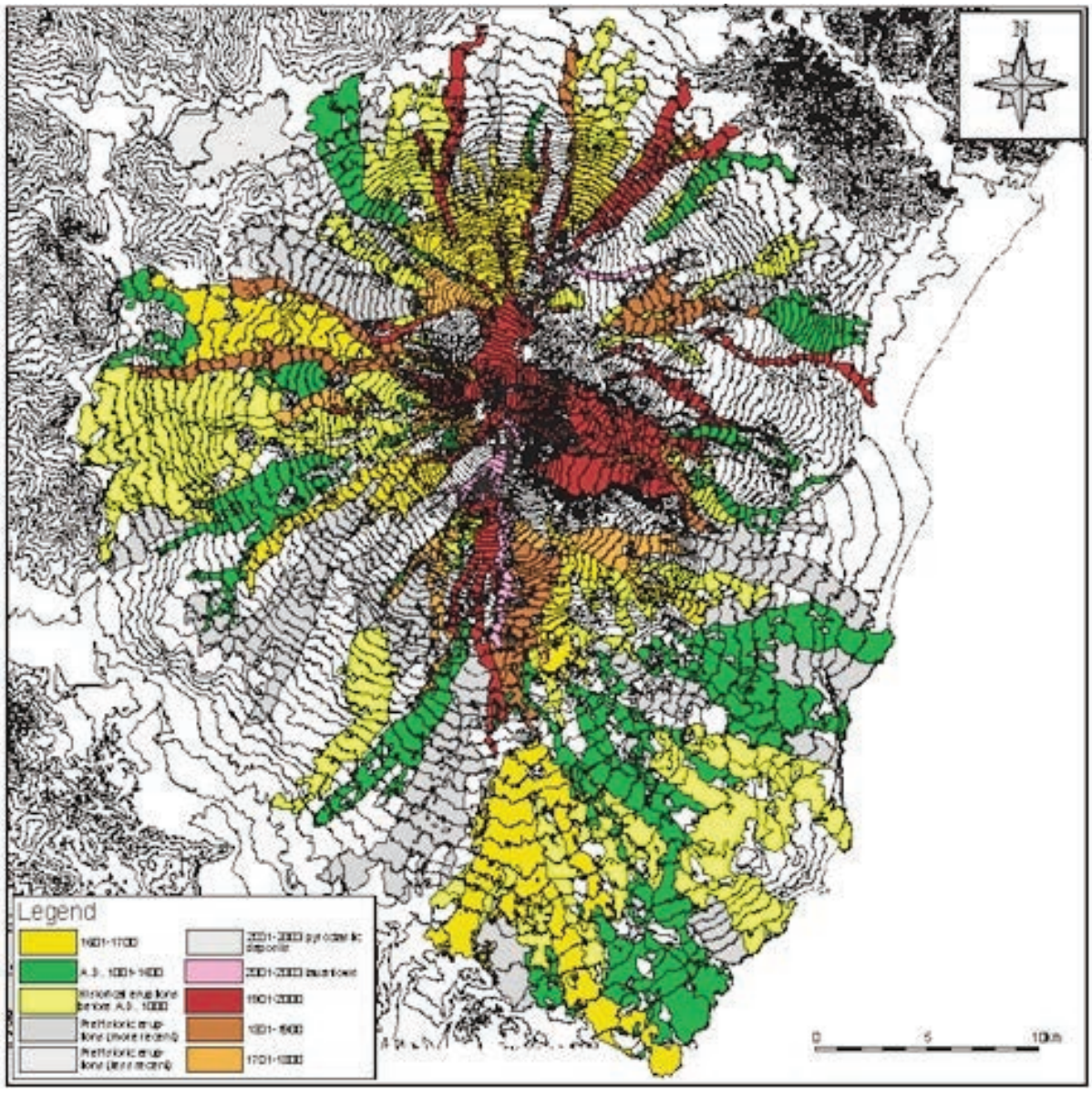

Figure 1A Distribution of historical and recent prehistoric lavas on Mount Etna.
Figura 1A Distribuzione di lave preistoriche e recenti sul Monte Etna.

Etna in times between flank eruptions, called "persistent" by Rittmann [1958]. It consists of relatively small Strombolian bursts accompanied, generally at distinct vents, by slow lava effusion (<1 m^3 s^{-1}). Before it started its exceptional series of lava fountains in 1998-2001, the Southeast Crater was the site of such "persistent" activity, and similar activity, accompanied by sporadic intracrater lava effusions, also occurred at the Bocca Nuova and the Voragine between 1995 and 1999. The Bocca Nuova itself produced a spectacular eruption in October-November 1999 with exceptionally strong Strombolian activity alternating with Hawaiian-style lava fountaining and copious overflows of lava onto the western flank of the volcano. Summit eruptions do not represent any significant threat to human property although episodic tephra falls generated by paroysmal events may cause damage to cultivated land and represent a nuisance to local residents. The map of Figure 1A shows the distribution of historical and recent prehistoric lavas on Mount Etna [Behncke and Neri ,2003b].

Flank eruptions, on the other hand, are distinct events that have occurred on an average of 4 years during the 20th century. Since they occur lower on the slopes, they represent a major hazard to human property and infrastructures, and out of the 25 flank eruptions of the 20th century, 10 have caused significant material damage, including the destruction of an entire village (Mascali) in 1928. These eruptions tend to occur preferably in certain sectors of the volcano, along more or less radially arranged fissure swarms, of which the most active are the South Rift and the Northeast Rift, with their respective fan-shaped fissure zones extending to the NNE and SE flanks [Acocella and Neri, 2003]. Out of the 15 flank eruptions that have occurred since 1971, 13 have occurred in these areas.

Flank eruptions were until recently believed to be mainly effusive, with only mild Strombolian activity at the source vents. The eruptions of 2001 [Behncke and Neri, 2003a; Billi et al., 2003; Lanzafame et al., 2003] and 2002-2003 [Neri et al., 2003] have shown that flank eruptions can be highly explosive: the latter of the two produced even more tephra than lava, which is extremely rare at Etna. In the long term flank eruptions are seen to occur in a cyclic manner [Behncke and Neri, 2003b]: rather than at random intervals, they occur in conspicuous clusters, or series, so that it can be assumed that in certain periods the volcano is more unstable than in others. Stable periods are marked by exclusively summit eruptions (and little seismic activity along the numerous faults criscrossing the eastern and southern flanks, which are affected by gravitational instability), whereas flank eruptions are frequent when there is also heightened evidence for flank instability. The latest flank eruptions, which occurred after a period of long-lived summit eruptions, coincide with a new period of flank instability, as was clearly seen during the 2002-2003 eruption [Neri et al., 2003].

It is now believed that the dynamics of Etna's volcanism are strongly controlled by the accumulation of magma below the volcanic edifice and flank instability [Acocella et al., in press]. Recent observations by Lundgren et al. [2003] indicate that flank instability is triggered by the rapid inflation of the volcano during sub-edifice magma accumulation, which, in turn, might be influenced by regional tectonics [Acocella and Neri, 2003]. It is likely that the voluminous accumulation of magma in sub-edifice reservoirs, the enhanced instability observed since 2001 and the unusually short interval between the flank eruptions of 2001 and 2002-2003 mark the beginning of a new eruptive cycle [Behncke and Neri, 2003a,b]. This implies that more flank eruptions will occur at brief intervals as long as the volcano remains unstable.

Geology of the measurement sites

This section briefly describes the geological characteristics of the sites where measurements were made. This is of particular relevance in the case of fieldspec radiance measurements, for which a number of sites with different characteristics were chosen, which are believed to represent the great variety of recent volcanic surfaces that is encountered at Mt. Etna.Generally there are two types of volcanic surface: lava flows and pyroclastic deposits. The earlier differ greatly in their surface characteristics, including their surface morphology ('a'a and p hoehoe) and vegetation cover, which in turn depends on (a) the age and (b) the location (elevation and exposure). Most lavas furthermore bear, to a certain degree, a pyroclastic cover that results from recent explosive volcanism at the summit craters (1990-2000) and from flank eruptive centers (2001 and 2002-2003). In order to obtain a record as representative as possible, sites were chosen on lavas on different flanks and of different age, and with pyroclastic covers that show different characteristics. The locations of the measurement sites are shown in Fig. 20 and Fig. 25. Special attention was dedicated to the products of the latest eruptions in 2001 and 2002-2003, which include voluminous and widespread pyroclastic deposits.The pyroclastic deposits were measured both at proximal and distal sites. They consist of lapilli-sized fragments in the earlier whereas ash is predominant at distal sites, as far as the eruptions of 2001 and 2002-2003 are concerned. Lapilli-sized scoriaceous fragments produced by short-lived paroxysmal episodes at the summit craters are abundant even at more than 10 km from their source and in many locations are mixed with the finer-grained pyroclastics of the 2001 and 2002-2003 flank eruptions. It is notable that re-working tends to affect much of these deposits within very short time after their emplacement and thus their characteristics

at the time of the measurements differ strongly from those to be encountered immediately after deposition, especially in the more distal locations.

Lava flows

The by far most abundant type of lava surfaces at Etna is 'a'a, with p hoehoe representing less than 10% of the exposed lava surfaces on the entire volcano. 'A'a lava is mostly of the blocky variety, with blocks ranging in size from a few centimeters to more than one meter. Flows (type A 'a'a) emplaced rapidly (a few hours to 1-2 days), at high effusion rates, are usually relatively thin (″ 2 m) and have flat surfaces with poorly developed flow channels and levees, and show less variation in the block size spectrum than flows whose emplacement occurred over longer time spans (>2 days) (type B 'a'a). These latter are also characterized by well-developed levees and often have conspicuous flow channels whose floor may lie up to 10 m or more below the lateral levees. Among the measured flows, the 1981 lava on the NNW flank was emplaced in very short time, whereas the 2002 lava near Piano Provenzana (NE flank), emplaced over a period of about one week, belongs to the most chaotic lava fields to be seen at Etna. Bulbuous p hoehoe, more rarely also ropy p hoehoe, occurs within some predominantly 'a'a flow fields in coincidence with ephemeral (tube-fed) vents and is particularly frequent in the 1983 flow field on the southern flank, especially in its central portion. Some lava flows, such as that of 2002 near Piano Provenzana, contain considerable quantities of welded scoriae that were deposited near the source vents and entrained with the flowing lava.

There are several lava fields on Mount Etna that are largely p hoehoe. In nearly all cases these are quite voluminous, including the 1614-1624 lava flow field, which was produced by the most voluminous historical flank eruption of the volcano (1-2 km^3). About 90% of the p hoehoe shows ropy surfaces, with bulbuous and slabby surfaces being much less common.

The development of vegetation on Etnean lava fields does by no means proceed in a homogeneous manner from site to site, but depends strongly on the surface characteristics, exposure, altitude and location of the respective site. From one area to the other there are strong differences even with similar flow surfaces and at the same altitude, because of the extreme microclimatic variations even at short distances. Generally the progess of plant colonization on p hoehoe is seen to take much longer than on 'a'a and is mostly due to the more compact nature of this lava type, which offers much less possibility for higher plants to take root. Lichens appear on both p hoehoe and 'a'a within about a decade after emplacement. Grasses and shrubs are more abundant in depressed areas, where their growth is often facilitated by the presence of pyroclastics.

Pyroclastic deposits

Contrary to the widespread notion of Mount Etna as a non-explosive volcano, pyroclastic deposits abound in many areas of the volcano and are not only restricted to near-vent facies (pyroclastic cones), but also occur even on many recent to sub-recent lava flows. A high percentage of these deposits is of fairly recent origin, coinciding with the much intensified summit eruptions since the mid-1990s and the strongly explosive flank eruptions of 2001 and 2002-2003. Although similarly explosive eruptions have also occurred in the past, Etna's eruptions throughout the 20th century have been remarkably non-explosive except for a number of paroxysmal eruptive episodes at the summit that became more numerous towards the end of the century. Distal pyroclastic deposits are rapidly reworked and are prone to disappear quite fast from lava flow surfaces, so that the current situation may be unusual unless explosive volcanism continues at a similar rate as in recent years.

Currently, three types of pyroclastic deposits can be encountered at Etna. One, the most abundant and long-lived, occurs close to eruptive vents where pyroclastic cones or spatter ramparts are built. In the case of relatively mildly explosive activity, these deposists consist largely of bombs and spatter which show varying degrees of welding, and although the constructs are relatively small (from a few to a few tens of meters in height), they are most resistent to erosion and reworking. The second is produced by more explosive activity and constitutes larger cones (up to more than 100 m in height) but individual fragments are generally smaller (lapilli with varying quantities of loose bombs) due to a higher degree of fragmentation. Where such cones are particularly exposed (such as those of 2001 and 2002-2003 on the upper southern flank), the finer-grained fraction is rapidly eroded, particularly by the near-constant and often gale-force wind. Significant degradation was observed at the cones of the latest eruptions very shortly after their formation and continues at an impressive rate. Runoff during heavy rainfalls is accentuated in areas where fumarolic activity leads to a local cementation of the pyroclastics and is capable of undermining the flanks and crater rims on these cones.

The third type of pyroclastic deposit varies from a relatively proximal to a distal facies and consists of continuous to discontinuous sheets mantling the pre-existing topograpy away from the cones themselves. It can be distinguished in two sub-types, of which one consists of lapilli-sized, highly inflated scoriae that are the products of extremely violent, short-lived episodes of lava fountaining at the summit craters. Deposits of this type are discontinuous except close (about 1 km) to the source and contain centimeter-sized clasts even at up to 10 km distance when freshly fallen; these fragments commonly break into smaller pieces during the many heavy rainfalls that occur at Etna. Nearly all of the presently occur-

ring deposits from lava fountains were produced in 2000, when the Southeast Crater produced 66 paroxysmal eruptive episodes.

In contrast, explosive volcanism during the flank eruptions of 2001 and 2002-2003 has produced deposits that maintain continuity far beyond the proximal areas. Closer to their source vents (but far beyond the pyroclastic cones themselves) they may be many tens of meters thick and reached thicknesses of dozens of centimeters even up to 5 km downwind from the vents. A characteristic decrease in the median diameter of the clasts is observed at increasing distance from the source, from lapilli-sized fragments within about 2 km from the vents to coarse ash farther away. On the downwind side such deposits were continuous at the time of deposition but much of the tephra was rapidly remobilized by rainfalls and removed from exposed sites whereas accumulation occurred in protected, depressed areas.

ISSN 1590-2595
Anno 2014_Numero 119

annex B

Sites surveyed by the spectroradiometer FiledSpec Pro

The location of the sites measured using the spectroradiometer FieldSpec Pro are described in Table 1B where the site name, its coordinates, the targets description and the date of the survey are shown. The different coloured cells indicates a certain number of targets referred to the same site,

Site	spectrum number	LAT	LONG	Description	Date
1 (Milo, Angelo Musco street, upward)		37,7328	15,1032	lava flow with compact and homogeneous lithoid horizon located at about 1 m underneath the lava flow surface	23/06/2012
	0-9			square with black regolith	
	10-19			low bush with small yellow flowers	
	20-29			Metric and submetric lava blocks with weathering and lichens	
	30-19			Broom	
2 (Milo, site in the opposite side of the road of 1)		37,7330	15,1034	very overgrown old lava flow with lichens and tephra covered blocks	23/06/2012
	40-49			lava block with lichens	
	50-59			Tephra	
3 (Milo, dirt road as 1 and 2)		37,7345	15,1032	lava flow with blocks covered by lichens and tephra. The vegetation coverage over the lava flow is medium.	23/06/2012
	60-69			black tephra	
	70-79			block with tephra and lichens	
		37,7336	14,8331	lava flow with pistachio trees	24/06/2012
	0-9			lichens covered lava block	
	10-19			lichens covered lava block	
	20-29			lava block totally covered by lichens	
	30-39			small pistachio tree + soil + pistachio tree branch	
5 (same site of 4)		37,7339	14,8331	lava flow covered by lichens in the middle of pistachio trees growing	24/06/2012
	40-49			lichen covered lava flow	
	50-59			same target of 40-49 spectra but different white reference	

Site	spectrum number	LAT	LONG	Description	Date
6 (Bronte: site close to the railway)		37,7882	14,8419	very weathered and lichens covered Pahoehoe lava with low bush and dry plants	24/06/2012
	60-69			lichens and moss covered lava block	
	70-79			lichens and mosso covered lava block with homogeneous and smooth surface	
	80-89			lichen covered lava block with rugged and irregular surface	
7 (south of Bronte: sp 280)		37,7614	14,8222	lichens and shrubs covered AA lava flow with lava tunnel structures	24/06/2012
	90-99			clasts and tephra	
	100-109			more lithic target respect to 90-99	
8 (road from Ragalna to Etna south)		37,6558	14,9765	lava flow 2001	24/06/2012
	110-119			lichens covered block	
	120-129			lichens covered block	
9 (road from Rifugio Sapienza to Nicolosi)		37,6969	15,0132	tehpra covered lava flow with outcropping lava blocks, moderately covered by vegetation with low shrubs	24/06/2012
	130-139			tephra covered lava flow	
	140-149			Tephra	
10 (road from Rifugio Sapienza to Nicolosi)		37,6860	15,0185	lichen covered lava flow	24/06/2012
	150-159			lichen and tephra moderately covered lava flow	
	160-169			lichen and tephra moderately covered lava flow	
11 (Forest Reserve road: south gate)		37,6919	14,9694	1780 lava flow with blocks covered by lichens	25/06/2012
	0-9			WR (white reference measure)	
	10-19			small blocks covered by lichens	
	20-29			lava and tephra	

Site	spectrum number	LAT	LONG	Description	Date
11 bis (Forest Reserve road: south gate, same lava flow of 11)		37,6928	14,9692	1780 lava flow as point 11	25/06/2012
	30-39			WR (white reference measure)	
	40-49			tephra with vegetation and sparse clasts	
	50-59			low shrub	
12 (Forest Reserve road)		37,7059	14,9624	2002 lava flow	25/06/2012
	60-69			WR (white reference measure)	
	70-79			black lava blocks with rugged surface and sparse tephra	
	80-89			black lava block	
13 (Forest Reserve road)		37,7226	14,9559	1942 AA scoriae lava flow	25/06/2012
	90-99			WR (white reference measure)	
	100-109			Scoriae	
	110-119			Scoriae	
14 (Forest Reserve road)		37,7295	14,9523	old lava flow covered with lichens and tephra	25/06/2012
	120-129			WR (white reference measure)	
	130-139			scoriae covered by lichens and tephra	
15 (Forest Reserve road)		37,7310	14,9514	old lava flow covered by several trees, bush and dry grass	25/06/2012
	140-149			WR (white reference measure)	
	150-159			low grass, lava and tephra	
	160-169			lava with tephra	
	170-179			Pine	
	180-189			spinosanto bush	
16 (Forest reserve road)		37,7575	14,9517	1999 lava flow with black scoriae	25/06/2012
	190-199			WR (white reference measure)	
	200-209			Scoriae	
17 (Forest reserve road)		37,8071	14,9391	old lava flow covered with lichens	25/06/2012
	210-219			WR (white reference measure)	
	220-229			small lava block covered by lichens	
18 (Forest Reserve road: north gate Pitarrone)		37,8148	15,0599	2002 narrow lava flow	25/06/2012

Site	spectrum number	LAT	LONG	Description	Date
	230-239			WR (white reference measure)	
	240-249			scoriae lava	
Etna North: Mare-Neve road					25/06/2012
Point 1CP (Etna North: Mare-Neve road)	etnanord_00_09	37,8541	15,0377	lava with blocks with strong surface weathering and lichens	
	etnanord_10_19	37,8541	15,0382	blocks lava with strong surface weathering and lichens as 00-09 and low dry shrubs	
Point 2CP (Etna North: Mare-Neve road)	etnanord_20_29	37,8549	15,0233	Basaltic lava outcrops with heaps of sparse regolith	
	etnanord_30_39	37,8547	15,0233	as 20-29 with some shrubs (basaltic regolith with low shrubs)	
Point 3CP Etna Nord Strada statale Mare Neve	etnanord_40_49	37,8543	14,9797	basaltic lava outcrop, no vegetation	
	etnanord_50_59			young basaltic blocks lava flow outcropwith very low vegetation	
Point 4CP (Etna North: Mare-Neve road)	etnanord_60_69	37,8564	14,9219	Very weathered lava blocks with vegetation and soil with very low plants	
	etnanord_70_79			as etnanord_ 60_69 but a little smoother and clearer	
	etnanord_80_89			as previous but more rugged	
Point 5CP (Etna North: Mare-Neve road)	etnanord_90_99	37,8547	15,0429	lichens covered lava block surrounded by vegetation	
	etnanord_100_109			as etnanord_90_99 with some moss cover	
UI	etnanord_110_119 etnanord_111_120	37,8466	15,0751	piece of polystyrene left on the road	
	etnanord_121_130			lava block	
	etnanord_131_140			heap of decimetric lava blocks and basaltic regolith with sparse bushes	

Site	spectrum number	LAT	LONG	Description	Date
	etnanord_141_150			lava block almost totally covered by dry moss	
19 (Paternò: "Salinelle" field		37,5730	14,8903	"salinella"	26/06/2012
	0-9			WR (white reference measure)	
	10-19 (aircraft upon the target)			whitish saline crust	
	20-29 (aircraft upon the target)			saline whitish crust	
	30-39			yellowish mud	
	40-49			yellowish little mud volcano with bubbling water	
	50-59 Radiance measurements (aircraft upon the target)			yellowish little mud volcano with bubbling water	
	60-69 Radiance measurements (aircraft upon the target Local Time 10:10)			1 m diameter water pool pozza	
	70-79 Radiance measurements (aircraft upon the target Local Time 10:10)			1 m diameter water pool pozza	
	80-89			whitish saline crust	
	90-99			WR (white reference measure)	
	100-109			same target of 60-79 where only radiance was measured	
	110-119			whitish saline crust	
20 (Paternò: "Salinelle" field west side)					26/06/2012
	120-129			WR (white reference measure)	
	130-139			greyish-whitish mud	
	140-149			whitish saline crust, the target is about 10 m far from the probe	

Site	spectrum number	LAT	LONG	Description	Date
	150-159			whitish saline crust with sparse small black blocks. Target about 10 m far from the probe	
	160-169			stretch of water, target about 10 m far from the probe	
21 (Paternò second site: mud and water volcanoes field)		37,5445	14,9196	small mud and water volcanoes, plain area with solid mud crust and structures mud cracks like	26/06/2012
	0-9			WR (white reference measure)	
	10-19			mud cracks	
	20-29			small bubbling pool with water and gas	
	30-39 (Radiance measurements)			small bubbling pool with water and gas	
	40-49			WR (white reference measure)	
	50-59			small grey mud flow	
	60-69			small mud flow and small gas bubbling pool	
	70-79			Water pool with whitish crust and further small bubbling pool inside	
	80-89			yellowish crust wit small cracks clay like	
22 (Sant'Alfio)		37,7384	15,1139	old lava flow covered by lichens, low bushes amd yellow flowers	27/06/2012
	0-9			WR(white reference measure)	
	10-19 (same target of laser scanning)			lava block surface	
	20-29 (same target of laser scanning)			lava block surface	
	30-39 (same target of laser scanning)			lava block surface	
	40-49			Bush	
	50-59			WR(white reference measure)	
	60-69			lichens covered lava block	
	70-79			dry bush	

Table 1B Locations of the sites measured with the Fieldspec Pro and descriprion of the measured targets.
Tabella 1B Siti di misura del FieldSpec e descrizione dei target misurati.

Index

Coordinamento editoriale e impaginazione
Centro Editoriale Nazionale | INGV

Progetto grafico e redazionale
Laboratorio Grafica e Immagini | INGV Roma

Via di Vigna Murata, 605
00143 Roma
Tel. +39 06518601 Fax +39 065041181

http://www.ingv.it

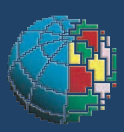

Istituto Nazionale di Geofisica e Vulcanologia